Piezoelectric/Triboelectric Micro Generators for Self-powered Autonomous Wireless Sensors

By

Sana Shakil

School of Chemical and Materials Engineering

National University of Sciences and Technology

2023

Piezoelectric/Triboelectric Micro Generators for Self-powered Autonomous Wireless Sensors

Sana Shakil

Reg.No: 317844

This thesis is submitted as a partial fulfillment of the requirements for the degree of

MS in Nanoscience and Engineering

Supervisor Name: Dr. Mohsin Saleem

School of Chemical and Materials Engineering (SCME)

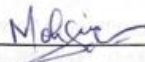**National University of Sciences and Technology (NUST)**

H-12 Islamabad, Pakistan

July, 2023

THESIS ACCEPTANCE CERTIFICATE

Certified that final copy of MS thesis written by Ms **Sana Shakil** (Regn No 00000317844), of School of Chemical & Materials Engineering (SCME) has been vetted by undersigned, found complete in all respects as per NUST Statues/Regulations, is free of plagiarism, errors, and mistakes and is accepted as partial fulfillment for award of MS degree. It is further certified that necessary amendments as pointed out by GEC members of the scholar have also been incorporated in the said thesis.

Signature: _____

Name of Supervisor: **Dr Mohsin Saleem**

Date: _____5- 09-2023_____

Signature (HOD): _____

Date: _____5/9/23_____

Signature (Dean/Principal): _____

Date: _____6 9 · 2023_____

NSC-07-2019

Dr. USman

Form TH-1
(Must be type written)

National University of Sciences & Technology (NUST)
MASTER'S THESIS WORK
Formulation of Guidance and Examination Committee (GEC)

Name: **SANA SHAKIL**

Department: **SCME**

Credit Hour Completed: **20**

NUST Reg No: **317844**

Specialization: **Nanoscience and Engineering**

CGPA: **3.17**

Course Work Completed

S/No	Code	Title	Core/Elective	CH	Grade
1	MSE-854	Characterization of materials	Core	3.0	B+
2	NSE-813	Essentials of Nanoscience and Engineering	Core	3.0	B
3	NSE-845	Nanolithography and Device Fabrication	Elective	3.0	C+
4	RM-898	Research Methodology	Additional	2.0	Q
5	MSE-856	Nano Material and Processing	Core	3.0	B+
6	MSE-872	Composite Materials	Elective	3.0	B+
7	NSE-847	Essentials of NEMS MEMS	Elective	3.0	B

Student's Signature

Date: **Nov 20th, 2020**

Thesis Committee

1. Name: **Dr. Mohsin Saleem** (Supervisor)   Signature: _____
   Department: **Materials Engineering Department**
2. Name: **Dr. Usman Khan** (Co-Supervisor)   Signature: _____
   Department: **SEECS, NUST**
3. Name: **Dr. Hamid Jabbar**   Signature: _____
   Department: **CEME, NUST**
4. Name: **Dr. Muhammad Aftab Akram**   Signature: _____
   Department: **Materials Engineering Department**
5. Name: **Dr. Muhammad Shoaib Butt**   Signature: _____
   Department: **Materials Engineering Department**

Date: 10/12/2020   Signature of Head of Department: _____

APPROVAL

Date: 11-12- 2020   _____
                      Dean/Principal

School of Chemical and Materials Engineering (SCME) Sector H-12, Islamabad

National University of Sciences &Technology (NUST)

MASTER'S THESIS WORK

We hereby recommend that the dissertation prepared under our supervision by Regn No & Name: __00000317844 Sana Shakil__

Title: __Piezoelectric/Triboelectric Micro Generators for Self-powered Autonomous Wireless Sensors.__

Presented on: __25 Aug 2023__   at: __1430 hrs in SCME (Seminar Hall)__

Be accepted in partial fulfillment of the requirements for the award of Masters of Science degree in **Nanoscience & Engineering.**

Guidance & Examination Committee Members

Name: **Dr Muhammad Shoaib Butt**   Signature: _____

Name: **Dr Muhammad Aftab Akram**   Signature: _____

Name: **Dr Hamid Jabbar** (CEME)   Signature: _____

Name: **Dr Usman Khan** (Co-Supervisor)   Signature: _____

Supervisor's Name: **Dr Mohsin Saleem**   Signature: _____

Dated: __29-08-23__

Head of Department
Date __29/8/23__

Dean/Principal
Date __19-8-23__

School of Chemical &Materials Engineering (SCME)

Dedication

I dedicate this thesis to my beloved Father and Mother.

Acknowledgments

All admiration to Allah Almighty. He is the One, who bestows and gives the power to us to think, utilize our expertise in knowledge in achieving remarkable solutions for mankind in every field. Therefore, I express my greatest thanks to Almighty Allah the universal and the architect of the world.

I like to express my gratefulness to my very supportive and respected supervisor Dr. Mohsin Saleem for his clear and patient guidance that directed me to fulfill my project and this thesis. His cool and calm behaviour motivated me to do my best. His valuable suggestions and feedback contributed to this thesis. Also, I am very grateful to all my GEC members who helped me and motivated me to do my best.

I would also like to thank my parents, family members, and my husband Sami Raja for their help, prayers, and their valuable suggestions.

I want to specifically thank Dr. Usman Khan for co-supervising my project and for his continuous support and motivation which helped me at various stages of my Master's.

I acknowledge the support provided by the Materials Engineering Department of SCME for providing me a platform to perform my experiments and use my skills in research work.

-Sana Shakil

Abstract

In recent decades, there has been a significant surge in energy consumption, predominantly fueled by the use of fossil fuels. However, this reliance on fossil fuels has resulted in a range of global issues, primarily due to the escalating carbon levels in the environment. To address the growing energy demand and mitigate environmental concerns, there has been a gradual global transition towards renewable energy sources. Through ongoing research and the persistent efforts of scientists, various materials have been developed to harness energy from previously overlooked sources, such as piezoelectric and triboelectric materials. Although only a limited number of these materials have been successfully commercialized, triboelectric materials have demonstrated significant potential for large-scale energy generation. This article focuses on the progress and experimentation involving a Hybrid Piezoelectric and Triboelectric Nanogenerator. The proposed study employed Bismuth Sodium Titanate-PDMS Composite as a Hybrid Piezoelectric and Triboelectric Material. The morphology was analyzed on Scanning electron microscopy. The phase analysis was done using X-Ray diffraction, which confirms its hexagonal structure. The chemical properties were observed by Fourier Transform Infrared Spectroscopy while vibrational modes of molecules were analyzed by RAMAN Spectroscopy. The electrical performance of the nanogenerator was tested by using a digital oscilloscope. The results showed that the output voltage of the nanogenerator reached at most about 23V and the output current reached around 46μA. With these results, they can be industrially perfected and commercialized. The continuous movement of water has the potential to be efficiently converted into energy, serving as a reliable source of electricity. Additionally, it can be harnessed to capture energy from human body motion and function as motion sensors. Through advancements in technology and ongoing research on triboelectric materials, we can effectively address the energy crisis.

Table of Contents

List of Figures

List of Tables

List of Abbreviations

PENG……………………………………………. Piezoelectric Nanogenerator

TENG……………………………………………. Triboelectric Nanogenerator

PDMS……………………………………………. Poly-Di-methyl-Silicate

BNT...…………………………………………. Bismuth Sodium Titanate

Chapter 1

Introduction

1.1 Mechanical energy harvesting

With the recent concerns about the energy crisis, we must find sustainable renewable energy resources that are environmentally friendly and contribute less towards carbon emissions [1, 2]. Extensive research has been conducted in recent years to develop renewable energy technologies, and mechanical energy harvesting is a good solution to our problem because it is a cost-effective alternative to traditional fuel sources. Until recently, mechanical energy harvesting was limited to the electromagnetic effect [3, 4], electrostatic effect [5-7], and piezoelectric effect [8-13].

An electromagnetic generator, which operates on the principle of electromagnetic effect, is in charge of converting mechanical into electrical output; however, it has the significant disadvantage of producing a low output voltage. Figure 1.1 depicts the device's structure and electrical output. The device, which consists of four magnets and a cantilever beam, can generate up to 10.82 W at a frequency of 58.5 Hz. An electrostatic generator, on the other hand, operates on the electrostatic effect principle. It generates opposing charges on two conductors, and mechanical motions using plates or drums can transport the charges to a high potential electrode.
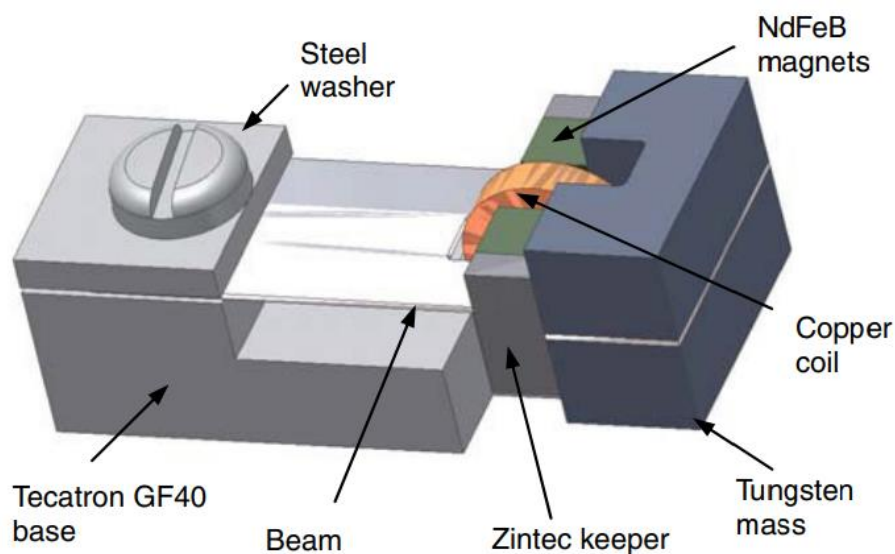
Fig 1. 1:A sketch of a typical electromagnetic generator[3]

One of the most popular varieties of these generators is the van de Graaff generator. In order to make the device smaller, an in-plane generator was created, as illustrated in figure 1.2. The device's power output was approximately 0.56 W. When the material becomes polarized when pressure is applied, a piezoelectric generator captures energy through mechanical strain. Common materials that have been utilized for this purpose are ZnO and PZT.
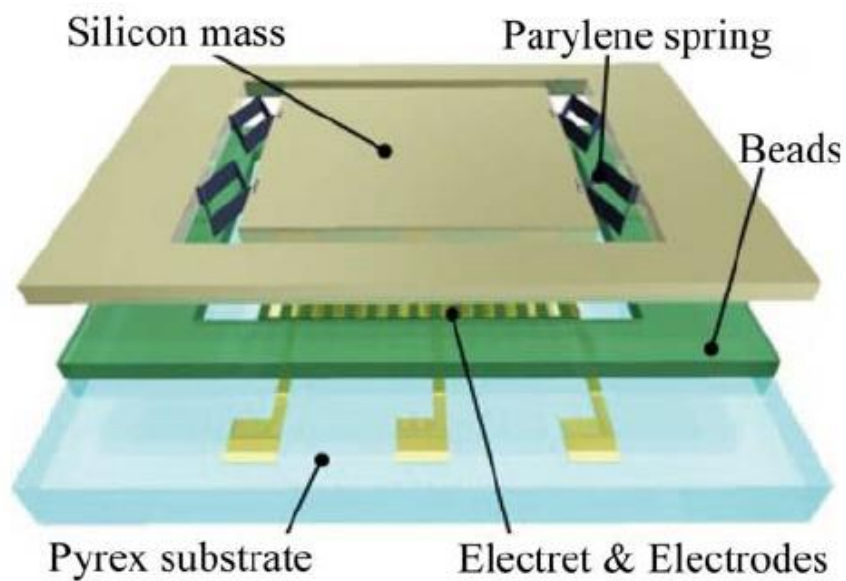
Fig 1. 2:A schematic of an electrostatic generator[5].

Although there has been a great use of these techniques, they are very likely to become less popular as they have the disadvantage of producing very low output voltage and when scaled to a lesser size, their output performance is affected which leads to the problem of not being able to miniaturize the device. When an improved structure is implemented with the use of superior materials to increase output, the cost of the device increases significantly, which is inefficient in the long run and limits its application as a sustainable energy harvesting device.

Numerous studies on the use of triboelectric materials in mechanical energy harvesting have recently been initiated. Triboelectrification is based on the production of opposite charges as a result of contact electrification between two different materials, and the device that uses this process to produce electrical power is known as a Triboelectric

Nanogenerator (TENG). TENG was originally introduced by the Wang research group in 2012 [14], and it generates electrical output when static charges are discharged [15]. They have an advantage over conventional mechanical energy harvesters in that they can harvest energy at low frequencies [16, 17]. There are numerous vibrations in our environment that are being wasted and might be exploited to harvest energy via TENGs, such as industrial machinery vibrations, road vibrations, ocean wave vibrations, and so on. To manufacture high performance TENG devices, several structures and designs have been examined. TENG's initial scope was limited to micro-scaled energy harvesting for use in electronic network applications, but its scope has gradually expanded into various important applications such as biological sensors, self-powered devices, actuators, and so on [18-23]. They have since been employed in motion monitoring devices, environmental sensing, and the internet of things. TENGs have been extensively researched as a means of harnessing blue energy and producing sustainable energy [24].

To harvest energy from the ocean wave vibrations, different designs were implemented including a floating TENG device which was proven to be quite efficient and hence provided a path for effective blue energy harvesting. There is massive energy in the ocean that can be harnessed to meet our future energy demands. The wave motions and tidal currents are quite easily utilized to produce energy with the help of simplistic TENG devices. Wind energy harvesting is also a great source of energy production and is considered quite sustainable but conventional windmills only work efficiently towards strong winds and the weak winds cannot be properly utilized to harness energy through windmills. This problem can be resolved by using TENG devices as they are effective towards low-frequency range energy harvesting including weak winds and weak ocean wave vibrations, which makes these devices quite the catch for next-generation energy production resources. Detailed introduction of triboelectricity and TENG devices have been thoroughly discussed in the next section.

1.2 Triboelectricity:

The term triboelectric derives from two Greek words, "tribo," which means rub, and "elektron," which means amber. The idea of triboelectricity has a long history, going back approximately 2400 years. It was initially identified when an amber and a cat's fur caused a spark when they came in contact [25-28]. Fundamentally, the triboelectric

effect occurs when two materials that have opposite charges on their surfaces come into contact with one another. The triboelectric effect typically occurs in insulators, particularly polymers like PDMS, Teflon, etc., although it can also be observed in some conductors like copper, aluminium, and other metals. The effect is not just restricted to interactions between solids; it also happens in interactions between solids and liquids and gases. Triboelectrification occurs in everyday life, such as when we contact a material and feel an electric spark, or when we rub a piece of paper in our hair and it later sticks to a balloon. The effect may also be observed in nature. For instance, when there is lightning during a rainstorm, the hails collide and generate static charges. When these charges are released, an electric spark is created [29]. Electrostatic charges are created as a result of the scattering of sand particles during a sandstorm, which also causes the phenomenon [30, 31]. Moreover, volcanic sparks occur due to the collision of ash particulates and hence triboelectrification [32].

Fig 1. 3:Triboelectricty in the environment. (a) Volcanic lightening during Chaitin volcano eruption, 2008 (b) Dust devil on Mars observed by Spirit rover, 2005 [31, 32]

1.3 Triboelectric Series:

There are many different types of materials that can be utilised to create TENG devices because practically any material can produce the triboelectrification effect. John Carl Wilcke originally described a triboelectric series in 1757, listing all the substances that can produce the triboelectric effect. Materials ranging from metals to polymers to even skin were included in the series based on their electron affinity, or capacity to loose and gain electrons [33]. According to Table 1, the materials near the top are positively

charged, while the materials at the bottom are negatively charged. The polarities of each type of material were determined by contact electrification experiments. A material at the bottom of the series will acquire a negative charge when it comes into contact with a material at the top, and the farther apart the elements are in the series, the better the charge transfer. The triboelectric effect is a contact-induced phenomena that is influenced by the total contact area of the surfaces and friction. It also depends on the choice of material and the surface shape of the materials. As a result, various surface morphologies, such as micro-pyramids, micro-needles, semi-circles, and cubes, have been used. By expanding the effective contact area and triboelectrification, these structures improve the triboelectric effect. There are numerous techniques that can be used to incorporate these surface morphologies into the material, including lithography, chemical etching, laser ablation, etc. The surface's potential can be considerably increased by chemically functionalizing it with various chemicals and nanoparticles. The properties of the material and, consequently, the triboelectric effect that is caused by it, can be impacted by the nanostructures on the surface. The substance utilised can be a composite; for instance, piezoelectric nanoparticles can be used to increase the materials' electrical output and permittivity.
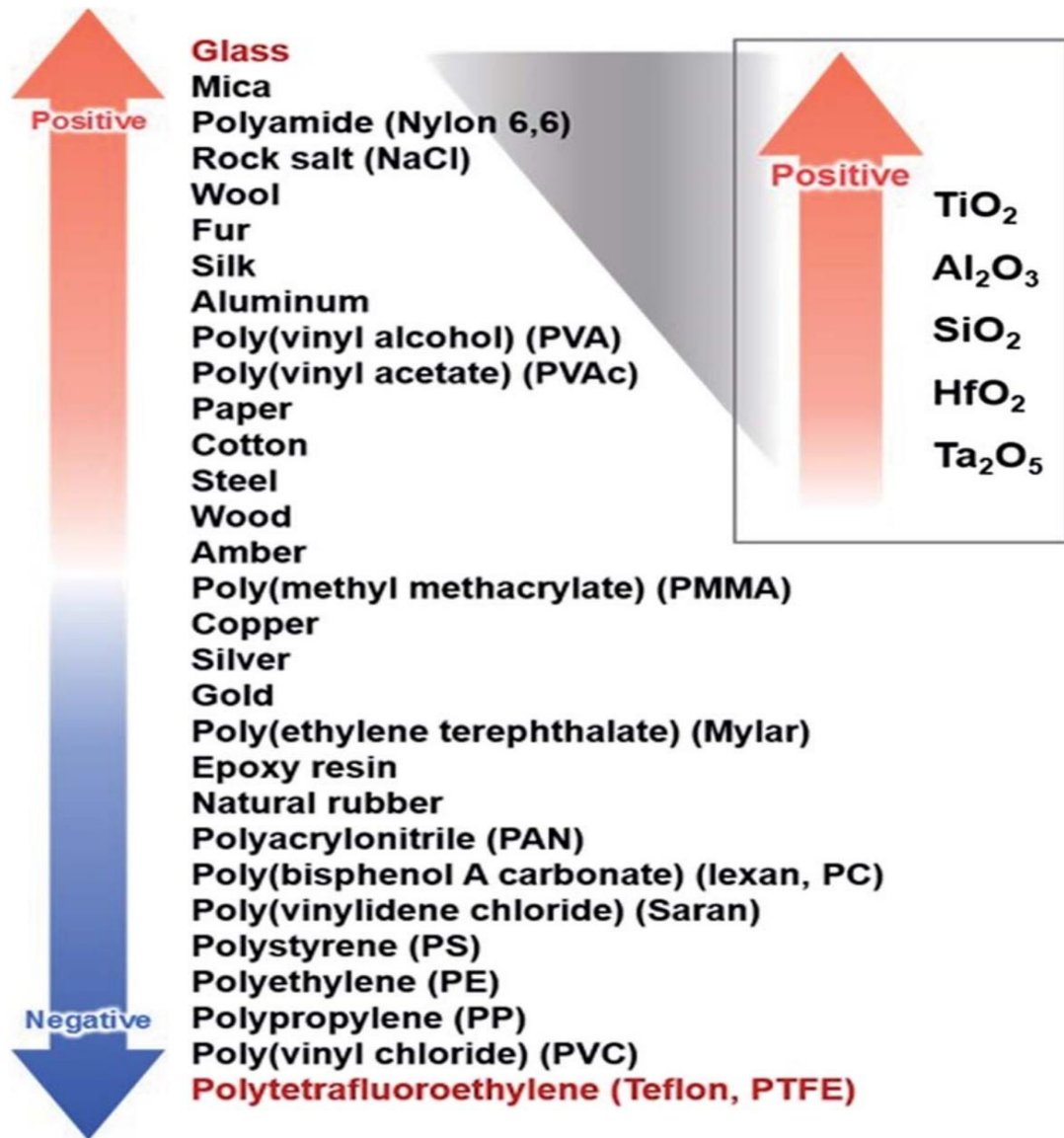
Fig 1. 4:Triboelectric series including the common materials being used, in order of their electronegativities [34].

1.4 Theory of Triboelectricity

Despite much research on triboelectric series, the theory underlying the action of triboelectricity remains difficult to understand, despite the fact that we encounter examples of it every day in our daily lives. The phenomena have been thoroughly studied by a number of researchers, including engineers, physicists, and chemists, but it is still not entirely obvious [35]. There has been much discussion about three distinct mechanisms that might account for it. The following are these mechanisms:

1.4.1 Electron Transfer

This mechanism focuses on conductors in which there is an exchange of electrons that occurs due to the difference in work function [36]. A work function "ϕ" is known to be an intrinsic property of a material and it is the minimum amount of work that is required to extract an electron from the solid. When two metals having different work functions come in contact with each other, a potential difference "Vc" is created between their surfaces due to which there is tunneling of electrons "e" that maintains the equilibrium again [37].

$$Vc = \phi2 - \phi1\ e \ \text{.......} (1)$$

Harper figured that the total charge transferred during this phenomenon can be calculated by considering it as a parallel plate capacitor [38]. The charge transferred "Q" can be obtained by the equation:

$$Q = CsVc \ \text{......} (2)$$

Where Cs is the capacitance.
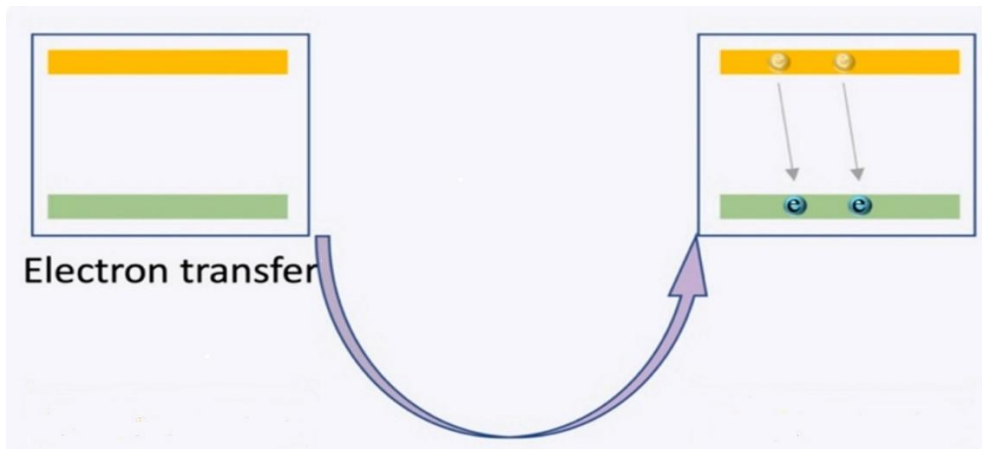
Fig 1. 5: Electrons are being exchanged due to the indifference in work function of the materials [39]

The process of triboelectrification begins when the surfaces come into contact with each other, which initiates charge transfer. When the surfaces separate, electron tunnelling stops after a particular critical separation distance, as shown in figure 1.5. As a result, the only process that can explain electron transfer as the cause of triboelectrification is metal to metal charge transfer.

This electron transfer explanation based on work function indifference cannot be used to metal-insulator/insulator-insulator interaction since insulators have a very wide band gap and so electron transfer is problematic [40].

When two insulators I_1 and I_2 come into touch with each other, the electrons in the first insulator's valance band cannot travel to the conduction or valance band of the second insulator because the valance states of the second conductor are filled. The researchers chose the surface state theory for this scenario, which claims that the surfaces of insulators have certain surface state levels and work functions, and electrons in different materials are transported within these states. The theory was then revived by Fabish and Duke, who proposed that the insulators have acceptor and donor states [41]. However, neither of these theories has experimental support, and neither has been definitively shown to be accurate [34].

1.4.2 Ion Transfer:

Research on electrophotography conducted in the middle of 1900s revealed that the surfaces of polymeric toners containing ionomers or molecular salts include both mobile and stationary, loosely bound ions with opposing polarity[28, 42]. As illustrated in figure 1.6, the mobile ions in one insulator can be transmitted to other insulators when they come into contact with one another. This finally results in the production of triboelectric charges in insulators.

Additionally, because non-ionic polymers cannot accommodate mobile ions, the ion exchange process is restricted to ionic polymers and cannot be extended to them. However, it was hypothesised that the hydroxide ions on the polymer surface may satisfy the need for mobile ions and make the ion exchange mechanism conceivable [43-45]. Contrarily, Baytekin conducted some studies and discovered that water is not required for triboelectrification but rather assists in maintaining the equilibrium of the surface charges. This finding contradicts the assumption that ion exchange may be the single cause for triboelectrification [46].
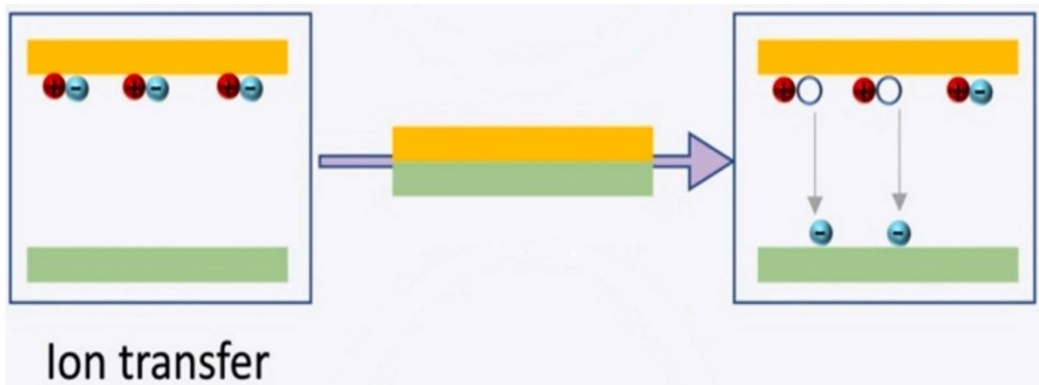
Fig 1. 6:Ion transfer Mechanism in which free ions are being transferred after contact [39]

1.4.3 Material Transfer:

According to this theory, friction caused by the rubbing of two material surfaces results in the transfer of micron-scale pieces of material that are charged because the shifted particles either came from bond-breaking or surface contamination, as shown in figure 1.7 [47]. The idea is considered to be inadequate since triboelectrification is a reproducible process, and hence material transfer cannot be the determining element because its extent decreases with each encounter [48]. In an effort to investigate this theory, Baytekin conducted some experiments in 2011 and found no evidence to support the notion that surfaces acquire opposing polarity. He proposed that positive and negative net charge distributions are produced by the mosaic of charges at the surfaces. He also carried out x-ray photoelectron spectroscopy, which indicated that material and charge transfer occurred throughout the triboelectrification process.
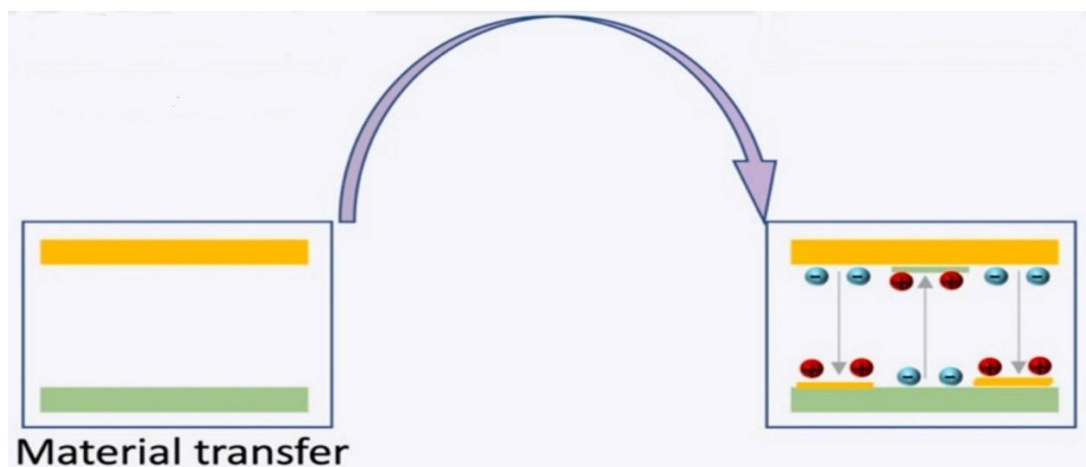
Fig 1. 7:Charge generation by material transfer mechanism [39].

1.5   Operation Modes of Triboelectric Nanogenerators:

Triboelectric Nanogenerators (TENGs) are devices that convert mechanical energy into electrical energy at both the micro and macro scales. They are utilised for energy harvesting as well as other purposes like motion detection and self-powered sensors. Depending on the application, many operating modes for TENGs have been proposed, such as having a freely movable TENG device structure. For the most part, TENGs are defined to operate in four different modes. These modes are further defined.

1.5.1   Contact separation mode:

The contact separation mode was the first introduced mode and is also regarded as the most basic [49]. Figure 1.8 illustrates the workings of this mode, which has a sandwich-like structure made of two layers of dielectric materials linked to an electrode. This way of operation involves applying an external mechanical force to bring one of the dielectrics into contact with the surface of the other dielectric, which causes the formation of charges on the surfaces of the materials. A potential difference between the electrodes attached to the dielectric layers is formed when the dielectrics are separated by a small distance. Electrostatic induction is a phenomena that occurs when the electrodes are externally linked to a load and an electron from the negatively charged surface begins to flow towards the positively charged surface, balancing the electrostatic field. The electrostatic potential would decrease and eventually disappear at the dull contact as the layers came back into contact as the electrons would flow back. Repeating this process would therefore cause an alternating current to flow through the externally applied load.

Triboelectrification happens not only in insulator-insulator interactions, but also in insulator-conductor interactions, as previously discussed. As a result, this working mode can be created by employing either two dielectric layers or two dielectric-conductor layers [50, 51]. The contact separation mode is the most basic of the modes; it consists of dielectric layers, electrodes, and an appropriate separation gap in a sandwich-like shape. Polymers are the most commonly utilised materials for this purpose because they have good triboelectrification properties and are located towards the end of the triboelectric series, giving them a great potential for becoming tribonegative; Teflon is a good example of this.
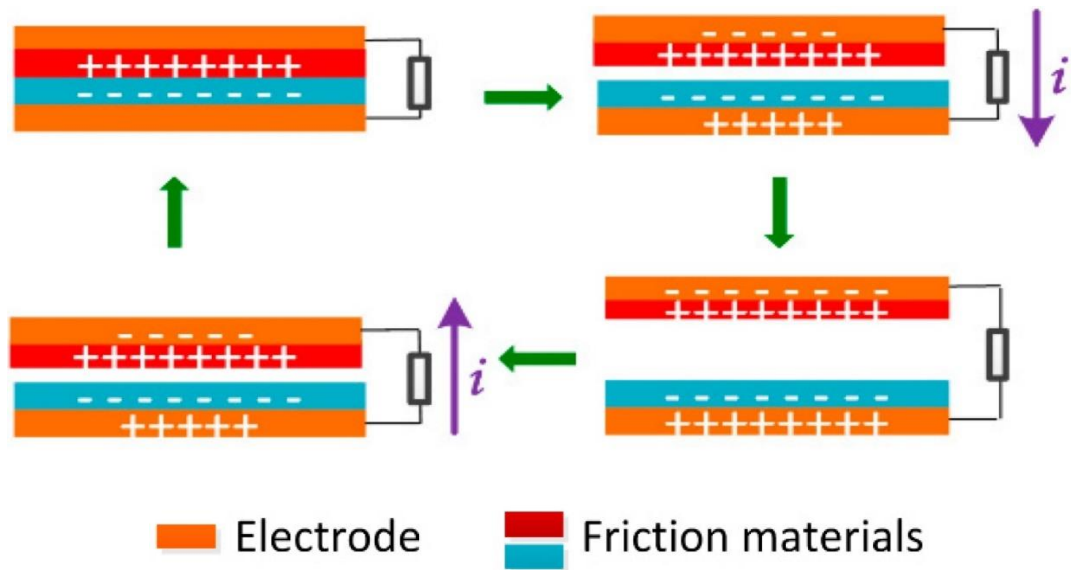
Fig 1. 8: Working mechanism of contact-separation mode [52].

Recent studies have shown that now inorganic materials, liquids, and chalcogenides can also be used for the TENG devices [53]. The electrodes used in these devices act as free electron sources and can be assembled with the dielectric layers in numerous ways.

For the attachment of electrodes to the dielectric, deposition and coating techniques can be used which can provide the closest assimilation, other than that adhesive conductive tapes can also be used to attach the electrode. The gap between the layers can be ensured by the use of springs, which would help the layers get separated automatically after the release of external force [51]. The gap can also be provided by using a curved structure for the layers[49].

1.5.2 Sliding Mode:

Figure 1.9 depicts the sliding mode, which consists of two surface layers in perfect contact with each other. In this mode, lateral sliding generates triboelectric charges rather than contact separation. The operation of this mode is such that when there is no separation gap, there are no charges since there is no potential drop, and when an external force is applied and surfaces are separated, there is the creation of triboelectric charges due to the potential difference between the surfaces.
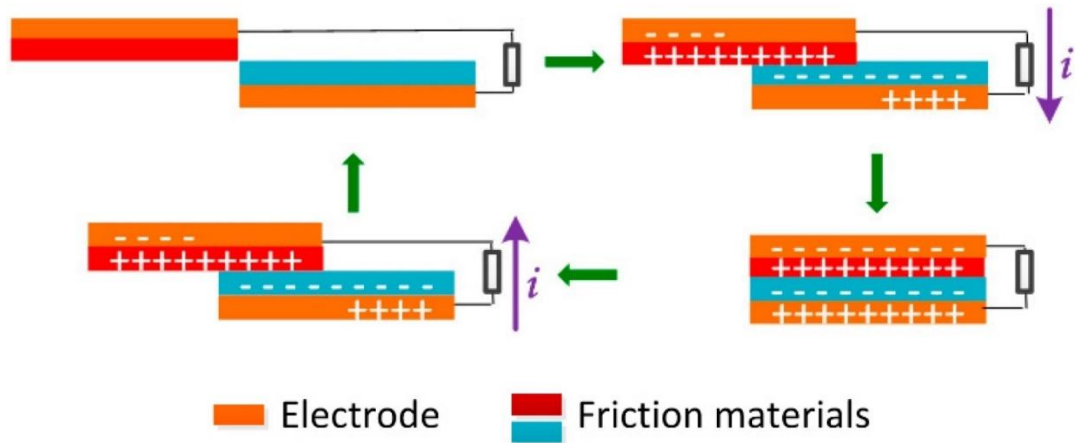
Fig 1. 9: Working mechanism of sliding mode[52].

Similar to the manner previously stated, the externally applied load would allow current to flow through the electrodes attached between them to balance the potential difference. Similar to how backward sliding of the surfaces would result in an oppositely directed current flowing through the electrode.

Theoretically, it was claimed that during this mode, the contact area lessens at the beginning and at the end of the cycle, though when tested experimentally, it was proven that this mode is a lot of efficient than the simple contact mode 65. This mode seems quite fit to be used for several kinds of motion including circular, rotational, and planar motion [54-57].

1.5.3   Single Electrode Mode:

We can use our TENG devices to generate electrical energy since we are aware that the triboelectric effect is an inevitable occurrence that happens in nature wherever there is mechanical contact between two surfaces. The two working modes previously outlined both make use of dielectric materials and compact layer-like structures, which are not ideal for capturing energy from the triboelectric charges that are present in our surroundings. In order to harvest the triboelectric charges from our surroundings, such as raindrops and human skin, the single electrode mode was developed specifically for this purpose [58-60]. The structure of this mode can consist of a freely moving dielectric material layer and a fixed electrode or an electrode assembled with a dielectric material, [61] as shown in figure 1.10.
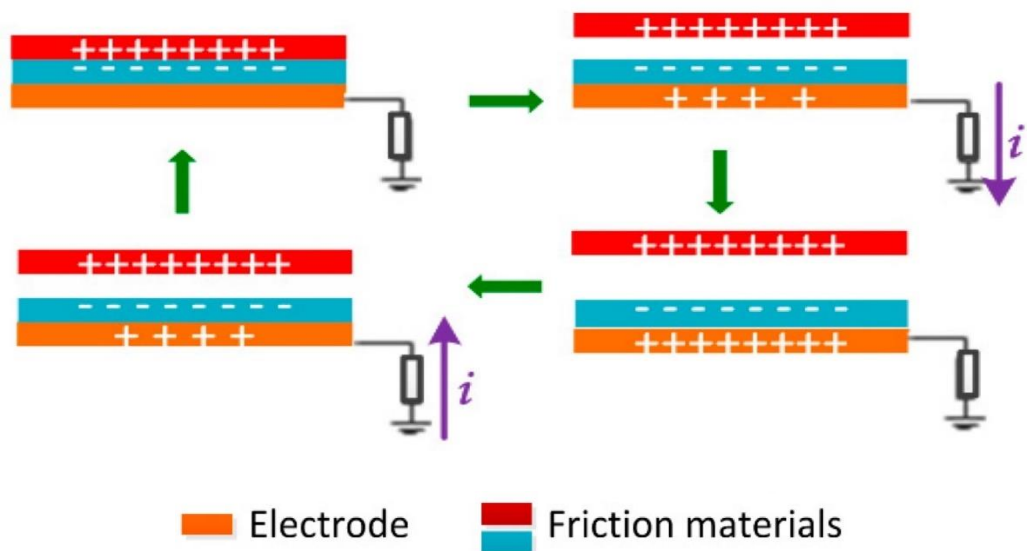
Fig 1. 10: Working mechanism of single electrode mode [52].

The electrode is attached to the fixed layer and grounded in the figure, which depicts the human skin as the freely moving surface that is coming into touch with PTFE. When the surfaces first make contact with one another, triboelectric charges are generated on their surfaces. When the layers are separated, there is a difference in the electric fields between the layers, which causes an electron flow through the electrode until the potential drop disappears. Again, the electrons would return from the ground to the electrode when the surfaces made contact with one another. The generation of electricity in an alternating direction would continue as long as this contact and separation process was repeated. The efficiency of this mode is significantly lower than the other modes despite the fact that a single electrode can effectively harvest the energy present in our environment [62]. This is because there is only one electrode being used, which limits the number of charges generated by the induction phenomenon.

1.5.4   Free Standing Layer Mode:

This mode is relatively similar to the single electrode mode that was previously addressed, but the structure is different enough that there should be one or more fixed triboelectric layers near to the current one [63]. The freestanding triboelectric layer is placed in this mode at a specified distance from the fixed triboelectric layers, and when these two layers come into contact and then separate, triboelectric charges are generated and a potential difference is established between them. As a result, electrons would travel through the electrodes and current would be produced. As triboelectric

charge generation can occur through mechanical contact with both conductors and insulators, the structure contains a fixed layer that may be an electrode coupled with a dielectric layer or a simple electrode [64]. The main benefit of employing this mode is that it can also harvest energy from the textile and large-scale motion industries [65, 66].
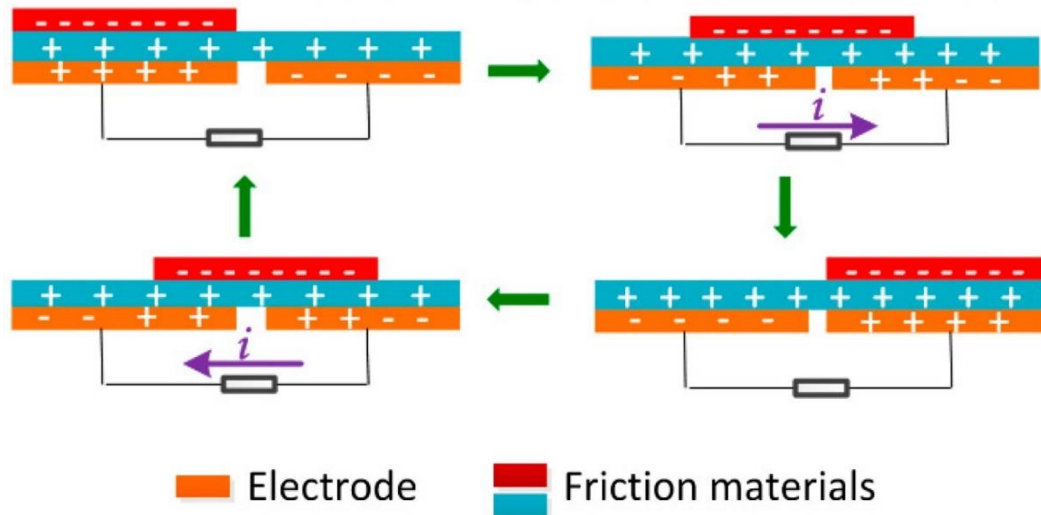
Fig 1. 11: Working mechanism of free standing layer mode [52]

1.6 Fabrication and Characterization of TENGs:

Since there are different TENG functioning modes, we can select the one that best suits the application for which it will be employed. Typically, in order to fabricate TENGs, we must choose materials from the triboelectric series and optimize the structure that we will use because it is important to the device functionality. We are aware that these nanogenerators use the processes of triboelectrification and electrostatic induction to convert mechanical energy into electrical energy. As a result, for the electrostatic induction effect, an increase in the number of induced charges is an important component for improving the output performance of the device. The key parameters to be taken into account when building the device construction are the gap distance between the surfaces, whether it is lateral or vertical, the time between contact and separation [67]. The TENGs have also been coupled with an electromagnetic generator in some study, which improves charge generation and output performance [68, 69].

Now considering the contact electrification step, the material selection, its surface morphology, and contact area are the elements that are to be well-thought-out to maximize

the number of triboelectric charges produced. As the output performance of TENGs is directly related to the density of triboelectric charges produced, we must choose a good pair of dielectric materials to enhance the efficiency of our device. To help with the selection of materials, the triboelectric series offers us several material choices and it is convenient to use as the materials are listed according to their relative polarizations which gives us an easy way to select our dielectric pair of materials. Metals, PTFE, PVDF, and PDMS are the most commonly used materials for the fabrication of TENGs as they lie at the ends of the series, as shown in the table.

Furthermore, there are various material requirements based on the application, such as water and chemical liquids for hydropower energy harvesting and chemical sensors [70]. Furthermore, numerous transparent, biodegradable, self-healing materials are used in the production of TENGs in a variety of applications [71, 72]. In addition to the intrinsic features of the materials, surface functionalization by chemical processes can be used to improve the triboelectric effect. Fluorination of surfaces via coating or plasma treatment is one method for increasing the negative polarity of the material [73].

Another way to increase the surface charge polarity is to use the cation and anion injection method, which could also lead to better output performance of the device. The surface charge densities of the dielectric materials are also dependent on the ambient environment in which the contact electrification occurs, thus the work done to increase the charge density gets wasted at some point. To deal with this issue, research has been carried out and it was found that if we use ionized air injection over the polymer surface, the molecules of the gas would sit on the surface and it could enhance the dielectric strength of the ambient atmosphere which would eventually maximize the surface charge density [74].

The active surface area of the dielectric materials that would come into touch with one another is the key characteristic that directly correlates with the output performance of TENG devices. The device's output current is directly proportional to the area of contact, which can be increased by increasing the device's size or by employing multi-layered devices [75]. In addition, altering the layer's surface morphology by applying various features to the surface can improve the surface contact area while simultaneously meeting the demands for size and dimension.

Chapter 2

Literature review

As the world is progressing with technology, the world's energy demands are also increasing day by day and we must start finding new resources to produce energy as we can't depend upon fossil fuels to extract energy anymore. Hence the world's first Triboelectric Nanogenerator was introduced in 2012 by Wang's group. It has great potential for harvesting mechanical energy from the environment that is being otherwise wasted and converting it into electrical power. TENG devices can be used in a lot of applications and due to their compact size and low cost, they can easily be used for human health care as well as shown in figure 2.1. For enhancing the triboelectric effect, different device structures, materials, and surface morphologies have experimented. Further mentioned is the work that has been done on TENGs.

Fig 2. 1:TENG applications in human health-care[76].

2.1 Health monitoring applications:

Further mentioned is the research that has been done in the field of Human Health Motoring:

- Zhu et al. created a self-powered TENG device for the shoe insole in 2013. As a triboelectric substance, he used PTFE [57]. Later that year, as indicated in figure 2.2, various improvements were made to the device. Because PTFE has some limitations, including limited flexibility, which overshadows its remarkable triboelectric characteristics [77, 78], it requires a folded structure. Even if we reduce the thickness of the material to get the needed flexibility, its mechanical strength is reduced and it will not be able to withstand the pressure created by walking. Hence, we cannot achieve our ideal properties using a thick PTFE layer and we would have to use a supplementary material e.g. Kapton, to obtain a springlike effect. The practical application of this TENG device in the shoe sole revealed an output voltage of 200V, while walking increased the current to 600mA. Even though the design and functioning mechanism are quite simple, it is a significant advancement in TENG technology for basic health monitoring reasons. However, this device can only detect torso movement and cannot quantify tiny body movement or interior physiological activity.

Fig 2. 2: a shoe insole TENG device with a folded structure that can light up LEDs on the application of pressure

- Wang et al. created a TENG device in 2014 to measure minor body motions such as internal physiological processes [79]. The device was an electronic skin with good flexibility, and PDMS was selected for this experiment because it is quite flexible and non-toxic, making it suitable for biomedical applications. We can also experiment with the layer's flexibility by reducing its thickness because it is just utilised for measuring pluses and throat vibration. The layer's thickness was set to 200 μm. The results demonstrated that the gadget could distinguish between normal and pregnant pulse movements, with an output current of up to 80 nA.

- In order to give a facemask a respiratory monitoring capability, Qixin Lu and colleagues created the TENG device for respiratory sensing (RS-TENG) in 2022. The RS-TENG is a compact, lightweight structure. FEP and aluminum foil were used as the triboelectric materials. In Fig. 1c, the RS-TENG's working mechanism is illustrated schematically. The air flow causes the FEP film and Al foil to come into contact when users inhale while wearing the smart facemask. The triboelectrification phenomena will cause an equal amount of different charges to be produced on each surface. As people exhale, the FEP film and Al foil will then separate. Due to electrostatic induction, there will be a potential difference between Al foil and conductive fabric tape.If wires were used to connect Al foil with conductive fabric tape, the potential difference would cause electrons to flow along the wires. Electric current is created as a result. The FEP film will grow nearer to the Al foil when they breathe in again, generating a reverse current. As a result, a regular current is produced when people breathe continuously. A maximum output voltage of approximately 8 V and a maximum output current of 0.8 μA [80] can be produced by the RS-TENG assembled on the facemask. The electrical impulses can be used to track a person's breathing condition and to diagnose certain respiratory conditions, such the COVID-19 pandemic.
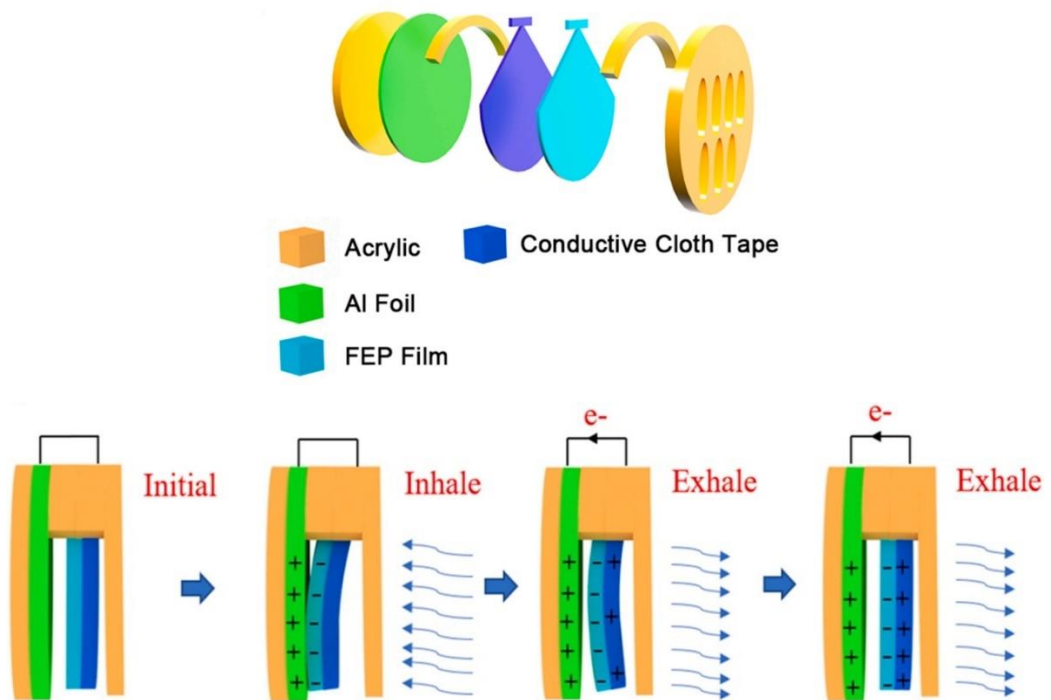
Fig 2. 3: Structure and working of RS-TENG device integrated on facemask

- In order to monitor human breathing information, such as rate and depth, Zhizhen Zhao et al. in 2016 developed a textile triboelectric nanogenerator (t-TENG) by integrating the as-made t-TENG into a chest strap [81]. They employed polyimide (PI) and PET (polyethylene terephthalate) as triboelectric materials. On a commercial sample weaving loom, it is made by directly weaving polyimide (PI)-coated Cu-PET (PI-Cu-PET) weft yarns and Cu-coated polyethylene terephthalate (Cu-PET) warp yarns. The contact area at each yarn crossing intersection changes as the gadget is lightly deformed by tapping or bending, which effectively generates triboelectric charges. The yarn crisscross intersections produce triboelectric charges to produce a maximum short circuit current density of 15.50 mA m-2.
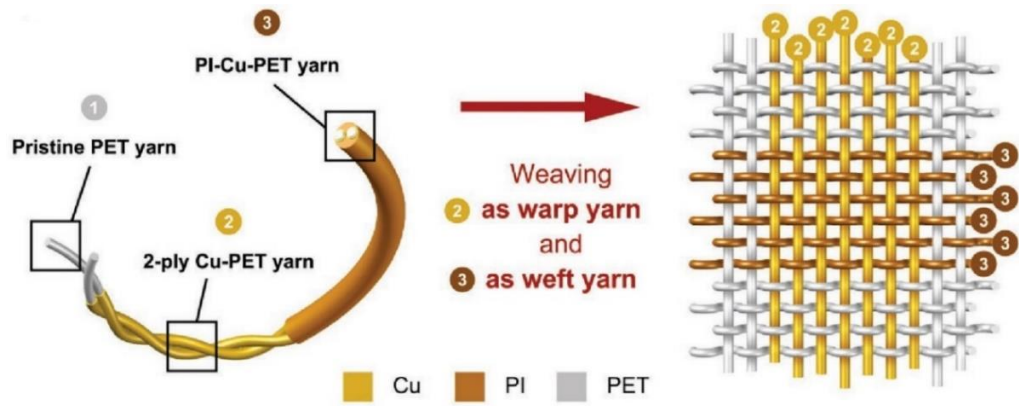
Fig 2. 4: TENG device with a woven structure

- In 2014, Yang et al. employed a flexible TENG device to be used for human machine interfacing motion monitoring [82]. They used PDMS as the tribonegative material, combined it with copper foil which was used as an electrode and the working mode used was the single electrode mode as shown in figure 2.5. For the PDMS, a pyramid surface morphology was employed to enhance its triboelectric properties and the enhancement of its output performance, as the research has suggested that pyramid morphology can induce better properties in comparison to the cubic structure[66]. The device proposed could be worn at the elbows or the shoulders and whenever there is contact between the PDMS layer and the human skin, a signal is produced due to which the motion is perceived. Finally, by using the Fourier transformation and the signal processor, we would be able to monitor the body motion. The results showed that the output voltage of the device reached up to 42 V, whereas the current density was calculated to be around 1μA/cm2. As this device has very high sensitivity, it really is a good innovation for the biomedical applications and helps us revolutionize the health monitoring. Similarly, we can also fabricate a patch type structure for the TENG device which has a similar assembly of the materials and it can be used for the measurement of physiological signals in vivo.
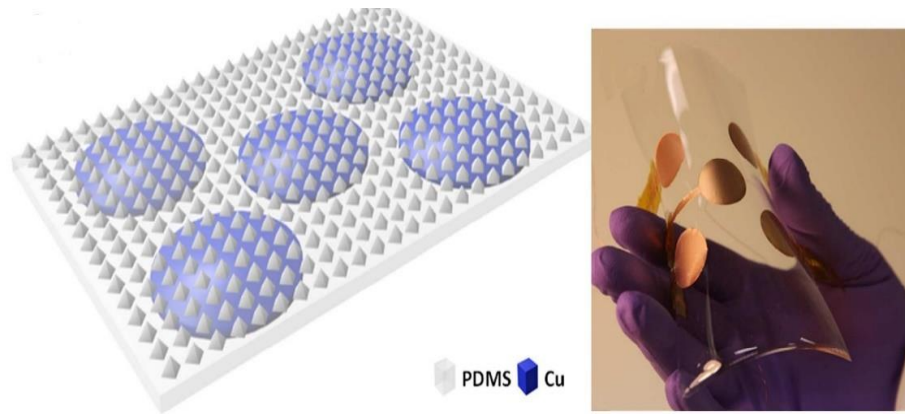
Fig 2. 5: TENG device with PDMS having a pyramid surface morphology[83].

- Bai et al. used FEP as the triboelectric material in the production of TENG for the pressure sensing application in 2014[83]. FEP can be used as a replacement for PTFE because it has similar qualities but also has several advantages over PTFE such as transparency, lightweight, and ease of manufacturing. Figure 2.6 shows how the device used the contact-separation functioning mode with the help of an arch design. The results showed that the device could sense the heartbeat and the breathing pattern and had a pressure detection resolution up to 0.34 Pa.

Fig 2. 6: TENG device with an arch design[84].

- Zhing et al. proposed a wearable TENG device in April 2012. He recommended using cotton thread coated with carbon nanotubes and PTFE to create a device with

a fiber-like structure. Experimentally the apparatus could detect body motion and utilize the mechanical energy to turn it into electrical energy, producing an output of about 0.1 W/cm2. The team used the same idea to construct a strain sensor as well[84]. It can be observed that by employing a design structure that resembles fibers, we can easily obtain a lot better flexibility because it reduces rigidity and makes contact separation easier. It alters the concept of having a full surface area into fiber elements, implying that our device is not limited by size and dimension constraints, making our work much easier for materials with relatively less flexibility. Although there are some issues about this structure because it only provides a line contact rather than a whole area contact, resulting in a lower output voltage. As a result, extensive research is required to get knowledge in this design framework. Although it is a novel concept, we must continue to work on having good flexibility as well as a large surface contact area.

- Yang et al. developed a TENG device in 2015 for the application of biomedical sensing devices [85]. They used Kapton as the triboelectric layer because it is a fantastic polymer with exceptional qualities such as biocompatibility, mechanical strength, thermal stability at high temperatures, and dielectric properties. As illustrated in Figure 2.7. The output voltage was 700V and the output current was 75 mA, which was outstanding.

Fig 2. 7: A TENG device with patch type design[86].

- Yang et al. simultaneously worked on two projects in 2015. In order to create a TENG device that could be attached to the throat for voice recognition reasons as

well as be utilized as a sensor for the human heart, they attempted to imitate the structure of the human ear-drum (as depicted in figure 2.8 [86]). They used the contact and separation working mode with PTFE and nylon as their triboelectric materials. The results revealed that the output signals were not particularly strong, but they were sufficient to carry out the tasks at hand. This experiment was the first to demonstrate the voice recognition capability in TENG, and it opened up a whole new world of applications for these devices.
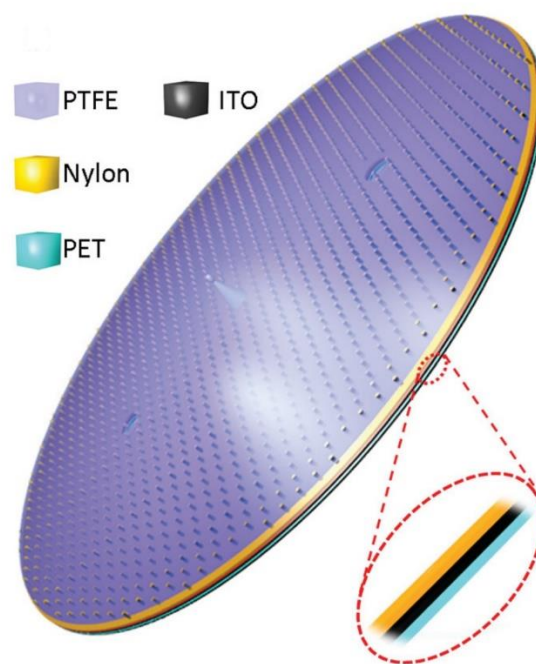
Fig 2. 8: TENG device inspired by human eardrum [87]

- In 2016, Li et al. suggested a TENG device to be used for heart monitoring, as shown in figure 2.9 [87]. The device going to be used inside the human body has to be very cautiously devised as it is going to get in touch with the inside of the human body. Keeping in mind the recent studies done on the TENGs, the device proposed had a multi-layered structure. The device employed PET, PDMS, and parylene as the main materials and they were encapsulated to achieve a flexible device having a good fatigue life. The device was tested by implanting it into a mice body and the results showed that an output voltage of 14V was achieved with

a current up to 5µA. Comparing these results with the other work done on converting the biomechanical energy into electrical energy, these results were up to 3.5 times higher.

Some months later, the team also devised another device that used PTFE as the triboelectric material and only the structure was changed to an arched design to employ the contact and separation mode. As given in figure 2.9 [84].
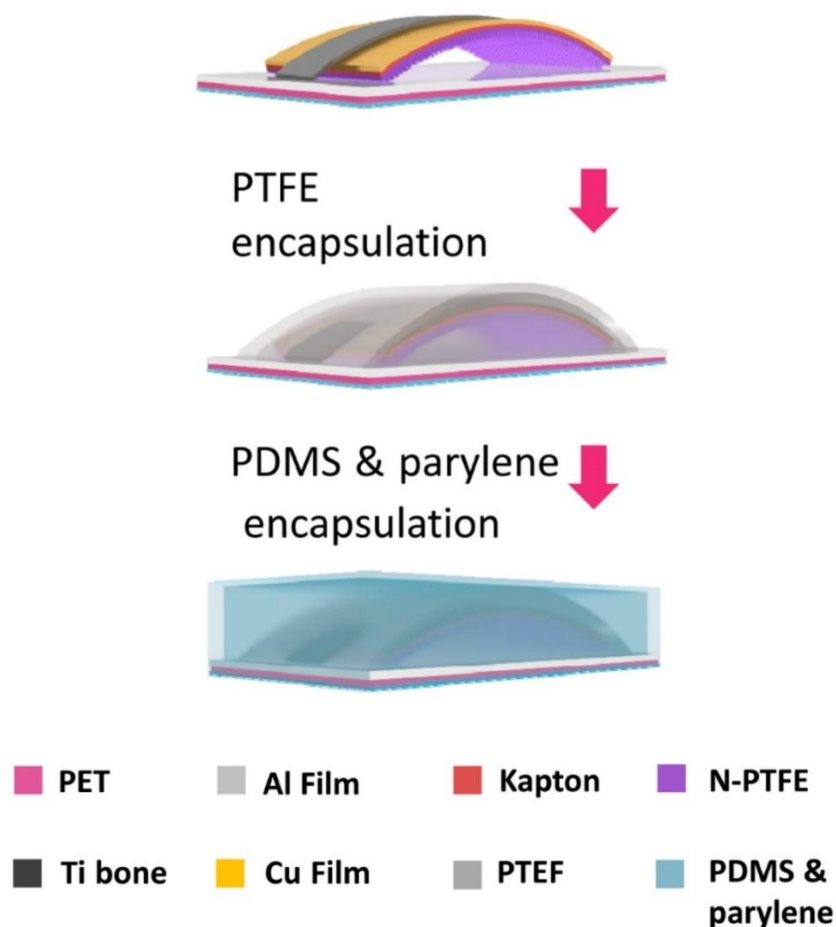
Fig 2. 9: TENG Device with a multi-layered structure to be used for heart rate monitoring[88].

- TENG devices are mostly made of solid materials, but we should attempt some liquid materials as well because they are more suitable for specific applications, hence some study has been done on making solid liquid TENG devices for

biomedical applications. In 2016, Yi et al. used a conductive liquid and rubber to create a TENG-like capsule, as shown in figure 2.10 [88]. The liquid did not contribute to the creation of triboelectric charge; it just acted as the electrode. In figure 2.11, the outcomes of this TENG device are shown. This device was a breakthrough in TENG technology because it was the first attempt to construct a TENG device employing a liquid phase of the material, even if it was only utilised for monitoring body movements.
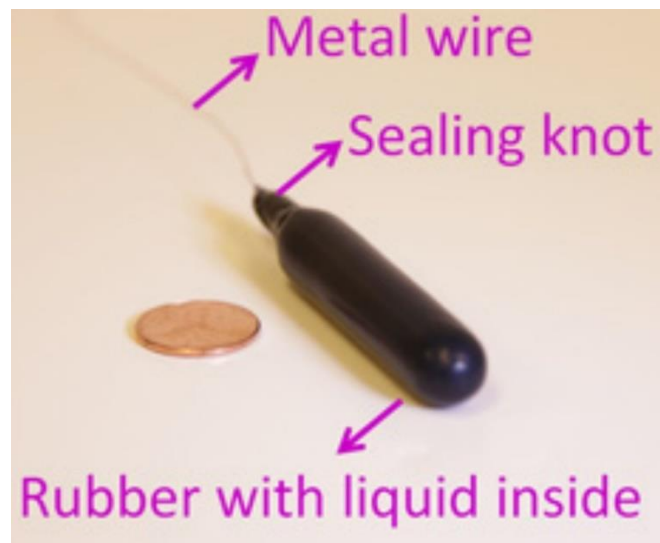
Fig 2. 10: TENG device employing a capsule like structure[89].
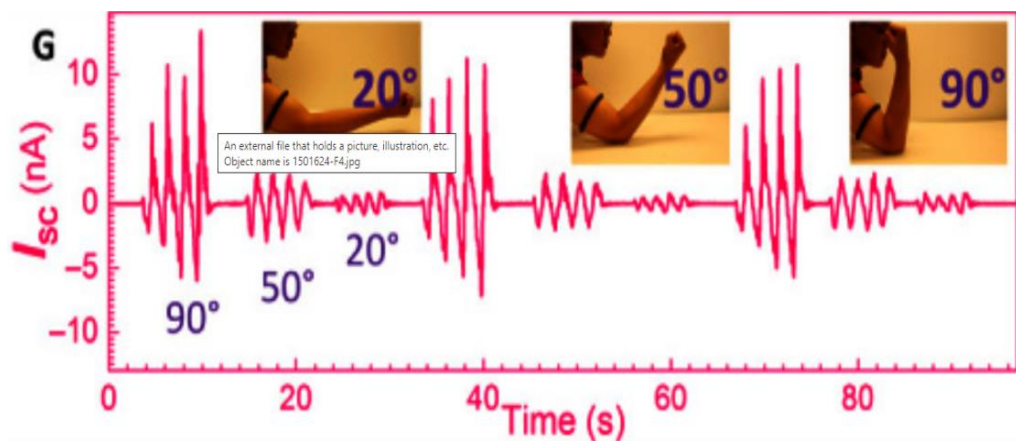
Fig 2. 11: Output current of capsule like TENG at different angles[89]

- In 2018, Lai et al. suggested a device based on eel skin, as depicted in figure 2.12 [89]. Later, [90] they developed a better version of the device, including nano-wires of silver wrapped around by PDMS, which resulted in increased flexibility and was used for human torso motion monitoring. Although the materials employed are not in liquid form, the interface is very similar to that of a solid-liquid interface. As a result, by constructing a non-full solid TENG, this work provided a new perspective on TENG devices.
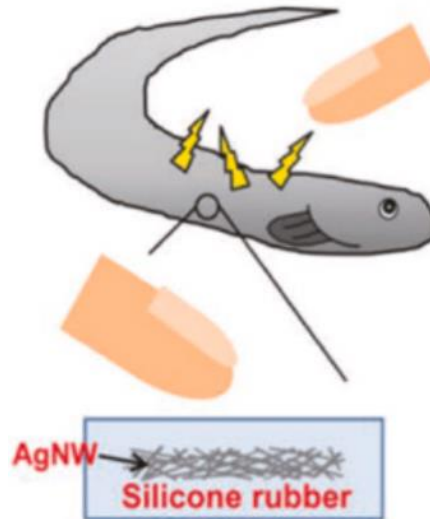
Fig 2. 12: TENG device with an eel skin like structure[90].

- In 2017, Shi et al devised a biomedical monitoring device that was self-powered and was able to attain wireless transmission and the results indicated that the efficiency of transmission was up to 26% with a distance of 1cm [91].
- In 2017, Ouyang et al. developed a sensor to monitor the antidiastole for heart disease. The results showed that the output voltage of 1.52 was detected and there was long-term working of the device and it was also quite inexpensive. For having enhanced properties, polyacrylamide-lithium chloride (PAAm-LiCl) hydrogel was used with PDMS to achieve a device with ultra-high flexibility. There has been a massive amount of research done on ultra-thin devices and up to 102 µm has been achieved[92].
- In 2017, Dong et al. developed a TENG device with a design of 3D woven TENG, fabricated with the help of fibers [93]. As shown in figure 2.13. The results showed that the device had its output several times better than the regular 2D textile TENG

device. The output power density came out to be 263 mW/m2 with a frequency of 3 Hz.
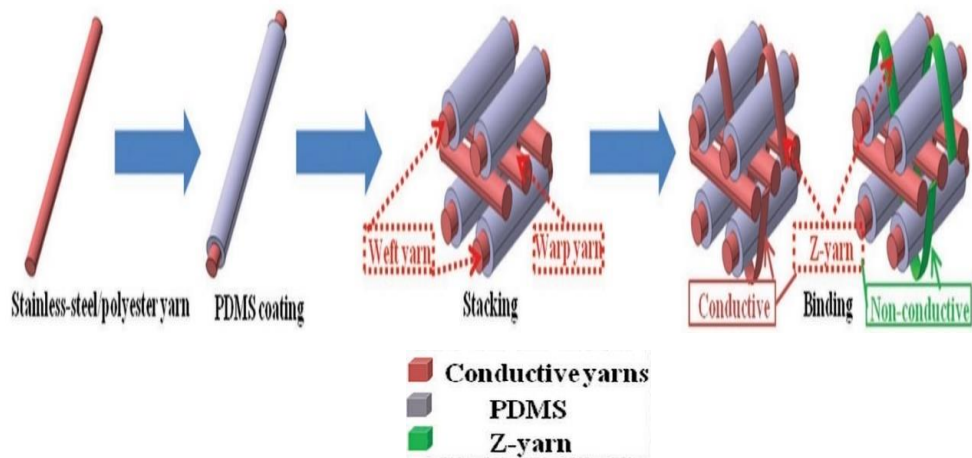
Fig 2. 13: 3D orthogonal woven TENG [94].

- Deng et al. created a TENG device with self-healing capabilities in 2018 [94]. It is possible due to the presence of covalent disulfide bonds in the elastomer matrix, which aids in the healing of fractures caused by thermal stimulation, as illustrated in the figure. However, this device's applicability is confined to torso monitoring only.
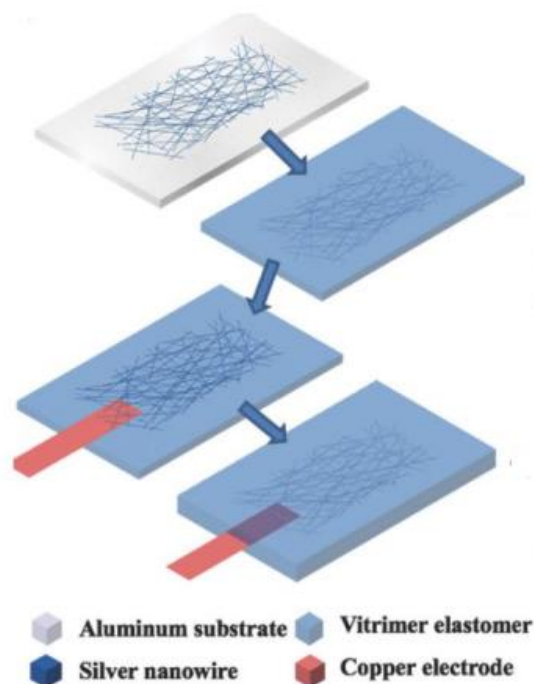
Fig 2. 14: TENG device with a self-healing structure[95].

- Meng et al. developed a TENG device to detect blood pressure in 2019. They used PTFE and PET as triboelectric materials, whereas ITO was used as an electrode material[95]. As illustrated in Figure 2.15. The device was made with a textile-like structure and a fibrous structure. The device is a technological breakthrough since it can measure blood pressure accurately in real time. We can have wireless communication of the BP and pulse rate when paired with the signal processor. The experiment findings showed that the device had a sensitivity of around 45.7 mV/Pa and a reaction time of 5 ms.
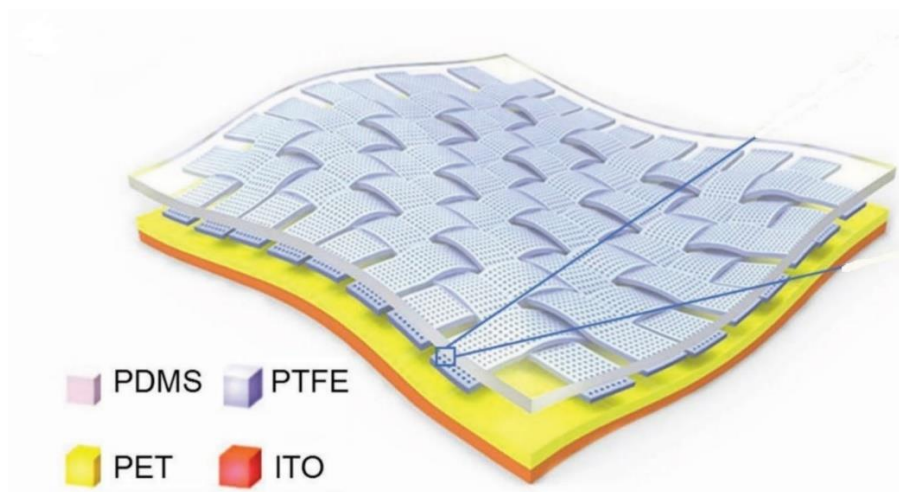
Fig 2. 15: Blood pressure sensor with an ITO electrode[96].

- Li et al. made a significant advancement in heart rate monitoring in 2019. They created a device and implanted it in a pig, as seen in figure 2.16 [96], utilizing PDMS and PTFE as the main materials. The output signal from the heart was strong because the materials employed have good triboelectric characteristics. The group also investigated how the plasma surface treatment affected the material, and they made sure that the output values were significantly improved as a result of the surface treatment. The device has a sensitivity of 1.2mV/mmHg and could track physiological signals. Although these devices are self-powered and do not require batteries, there are still problems with device life because of their fatigue life.
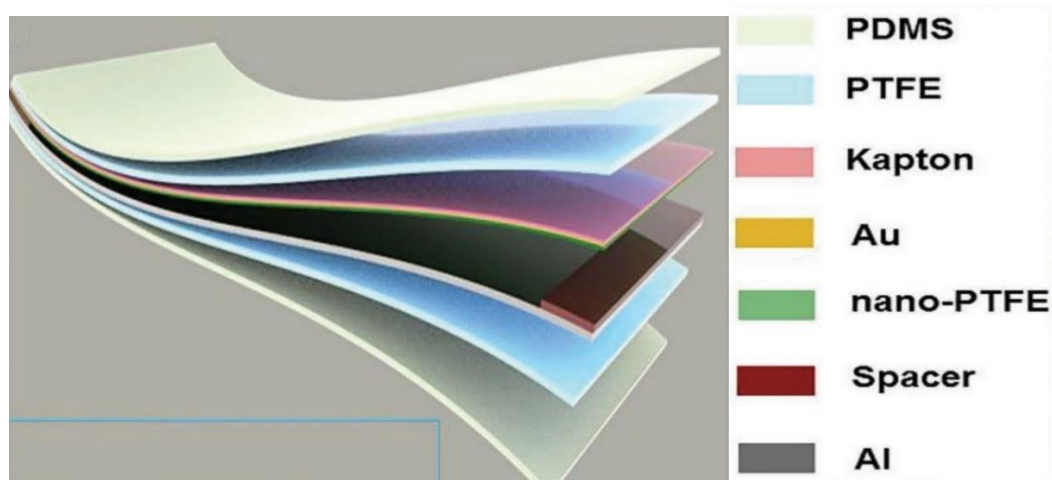
Fig 2. 16: Heart-beat monitoring TENG device[97].

- A transparent and stretchable TENG device was created by Zhao et al. in 2019 and is depicted in figure 2.17 [97]. The team used PDMS as the contact layer and a poly(2-acrylamide-2-methyl-1-propane sulfonic acid) (PAMPS) ionic gel layer. There are no other materials added because the device is simply used for sensing; nonetheless, the PDMS used had a patterned surface to improve the triboelectric characteristics and have better contact and separation. Experimentation on the device revealed that sensitivity in the range of 0.1-1 N was around 0.39-1.46 V/N. Taking inspiration from the leaf shape of C. zebrine, the material used a cone-like structure to improve sensitivity in the PTFE-based device results, which were nearly 14 times better than flat-surfaced PTFE [98]. Similarly, the objective of adopting a textile-like structure in electronics is to improve the sensitivity of device as well as its flexibility.

- In March 2020, Fan et al. fabricated a TENG device using a textile design. The results showed that the sensitivity of the device was around 8mV/Pa, it had a great response time of 20 ms, the device was still stable even after 100,000 cycles, and had a wide range of frequency bandwidth. The device was able to monitor arterial pules and respiratory signals.
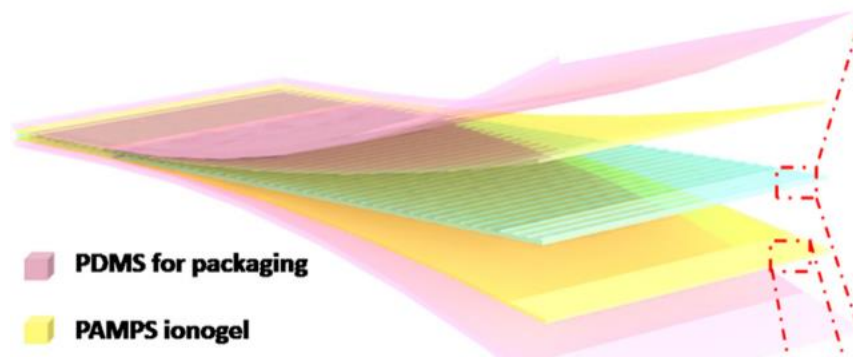
Fig 2. 17: Transparent and flexible TENG device[98].

Herein, we have summarized all the important research that has been carried out on TENG Devices for the applications of human health monitoring.

2.2 Human Health-Care applications:

- In 2013, Yang et al devised a new kind of TENG device that was built into clothing. As shown in figure 2.18 [20]. They employed PDMS and Al as the contact layers and used the contact and separation working mechanism and the thickness of the device was around 0.8mm only. They also performed some surface treatments to see the performance of it on the output performance. The experiment showed that a voltage of 17V was achieved from normal walking and the device was able to light up almost 30 LEDs. Comparing the built-in clothing TENG devices with the ones in shoe soles, the shoe ones have limitations on the size and dimensions but they are usually simpler to work with and can harvest energy from walking.
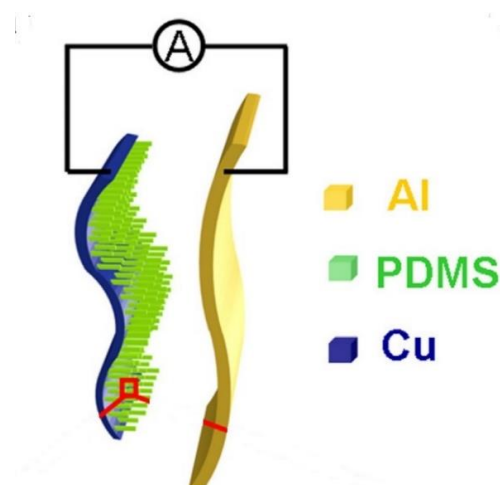
Fig 2. 18: Cloth in built TENG device[21].

- • Lin et al. created a textile TENG array to track human sleep behavior in 2018. The textile TENG is made of conductive fibers and PET, which is a triboelectric substance. The top and bottom textiles were laminated with conductive fibers, and wavy-structured polyethylene terephthalate (PET) films were sandwiched between the top and bottom fabrics. The textile TENG has a pressure sensitivity of 0.77 V Pa^{-1} and a response time of less than 80 ms. [99]. When a sleeper lies down on the textile TENG-based smart mattress, the sleeper's body posture, position, and pressure distribution can be gathered in real time. The information gathered from the sleeper can be used to evaluate sleep quality and provide a comprehensive dataset for the diagnosis of sleep disorders such as obstructive sleep apnea.
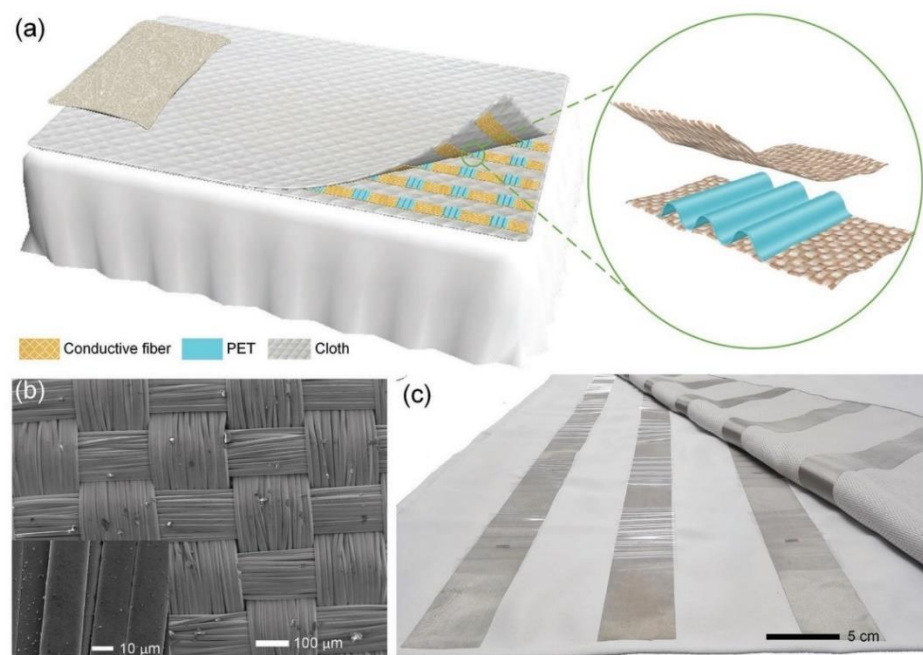
Fig 2. 19: TENG device having a wavy structure [99]

- A TENG device for use in the shoe sole was created by Yang et al. in 2013 and is depicted in figure 2.20 [100]. The device was constructed using PDMS with PET as the contact layer. The PDMS has certain designs on the surface, and ITO was used as the electrode material. ITO has great electrode qualities because it has outstanding electrical conductivity and transparency, making it suitable for use as a wearable device. Due to its exceptional properties, it has

grabbed the attention of researchers. According to the experimental results, the device can attain a high voltage of up to 220 V and a current density of roughly 0.8 A/cm2. The device was capable of lighting nearly 30 LEDs, and the voltage was high enough to power some small electrical devices, such as a glucometer. Among the group's prior work is a combination of TENG and backpack for sustaining vibrational motion while walking [101]. Another group used a similar design structure to create a compact, lightweight self-powered device.
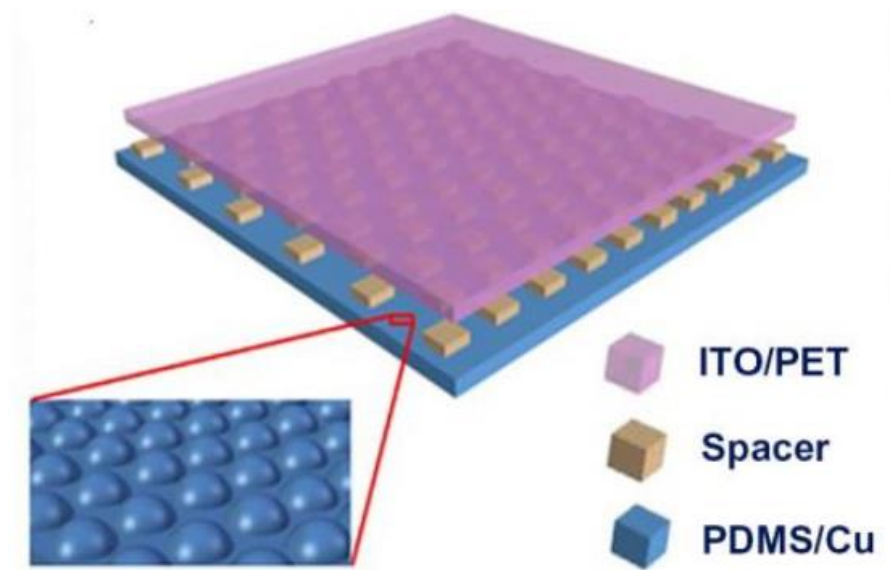
Fig 2. 20: TENG device to be used in shoe sole [101].

- Li et al. made a breakthrough in the field in 2014 by creating a TENG device that can capture both physiological and mechanical energy from humans. Figure 2.21 [100] depicts this. It was the first time a TENG device harvested energy in vivo. The device's mechanism was good, as it could harvest energy from respiration and use it to power the pacemaker. The triboelectric materials for the TENG device were Al foil and PDMS, with the PDMS having a pyramid surface shape to improve electrical output. Gold foil and Al foil were utilized for the electrodes. To isolate the device from its environment, it was encapsulated with a polymer.

The device was evaluated by implanting it within the rat's body under the left chest skin. During the mice's inhale and exhale, the thorax contracted and

expanded, causing deformation for the TENG device, which resulted in the generation of electrical output. The results showed that with a current of 0.14mA, an output voltage of 3.73V was obtained. From a theoretical standpoint, five breaths were enough to activate the pacemaker once.
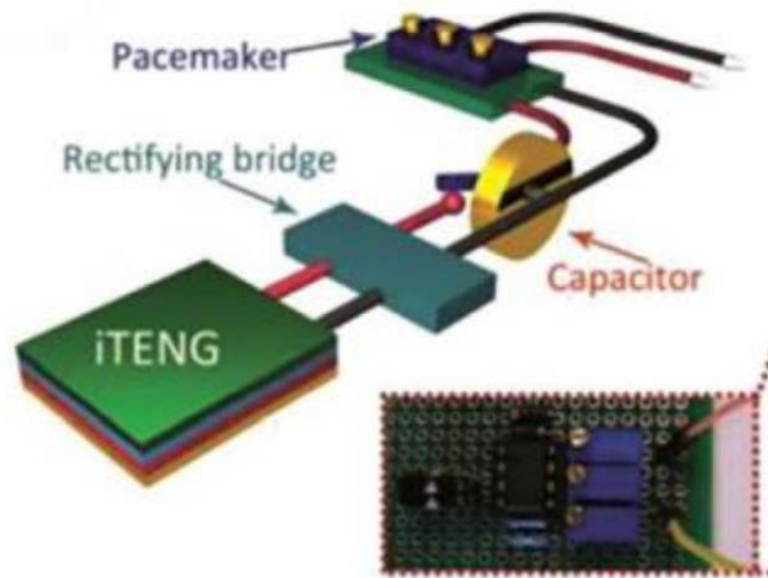
Fig 2. 21: Structure and design of self-powered pacemaker[101].

- In 2016, Zheng et al. fabricated a biodegradable TENG device for the very first time[102]. The device was able to power two micro-grating electrodes to orient the never cell growth and then it was able to get degraded and absorbed into the body after finishing its purpose, and it had no side effects.

- Song et al. created a self-powered TENG device that was to be implanted into the body and used as a drug delivery system [103]. As illustrated in Figure 2.22. The triboelectric material was PTFE and copper, and the operating mode was the freestanding triboelectric layer mode. The triboelectric layers provided the electrical energy required for ionization, and the bubbles generated as a result expelled the drugs for delivery. The flow rate of the medicine could be changed experimentally by varying the speed of the device. Even though the

device is far from being used in practice, it does present a novel method of TENG device application.
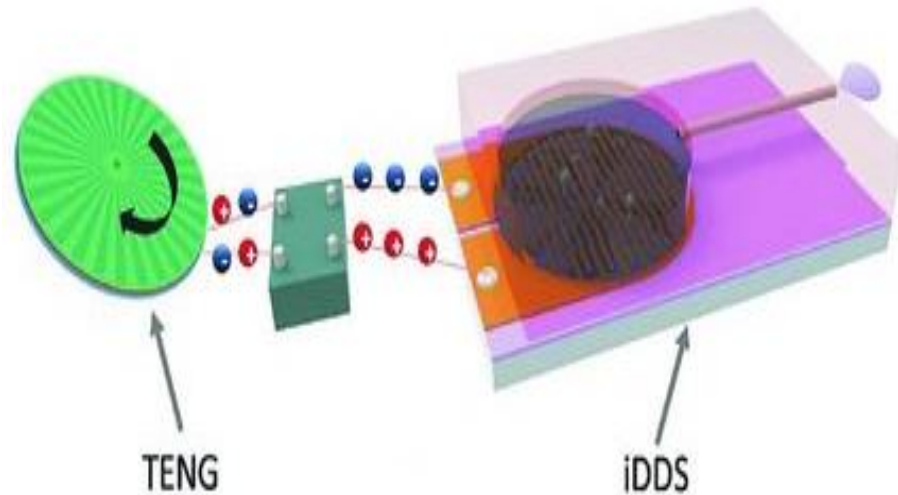
Fig 2. 22: Self-powered implantable drug delivery system [104].

- Lin et al. developed a self-powered sensor with a contact sliding mode in 2017 [104]. As illustrated in Figure 2.21. An elastic was used for the sliding mode, and the triboelectric materials used were PTFE and Cu foil. Although this functioning mode is less effective because it results in lower output voltage, it was a rare attempt that was successful. According to the results, an output voltage of 540 V was obtained. When worn on the body, the device was able to harvest energy from walking, with a conversion efficiency of up to 58%. Lin et al. developed a self-powered sensor with a contact sliding mode in 2017 [104]. As illustrated in Figure 2.21. An elastic was used for the sliding mode, and the triboelectric materials used were PTFE and Cu foil. Although this functioning mode is less effective because it results in lower output voltage, it was a rare attempt that was successful. According to the results, an output voltage of 540 V was obtained. When worn on the body, the gadget was able to gather energy from walking, with a conversion efficiency of up to 58%. It can deliver real-time heart rate information when attached to a sensor and a Bluetooth communication circuit.
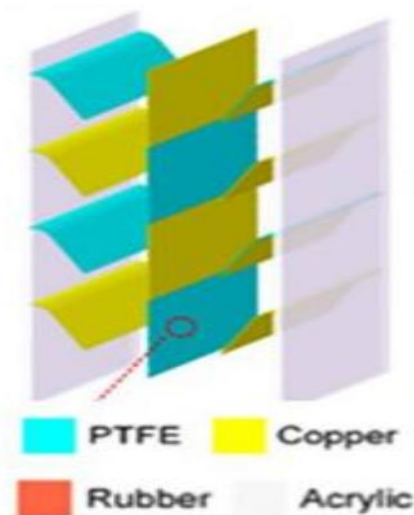
Fig 2. 23: TENG device with a contact sliding mode[105].

- In 2018, Jiang et al. succeeded in merging MXene electrochemical micro-capacitors with TENG, making the device more wearable due to its compactness [105]. The TENG was made of silicone rubber and carbon fibers, and the operating mechanism was a single electrode mode. As illustrated in Figure 2.24. The device attached to MXene made use of its extraordinary qualities, and the entire device could be worn as a bracelet, with the output being sent to an electronic watch. According to the results, an output voltage of roughly 50 V was obtained with a current density of 0.12mA/cm2. The device could assess pulse and blood pressure in real time.
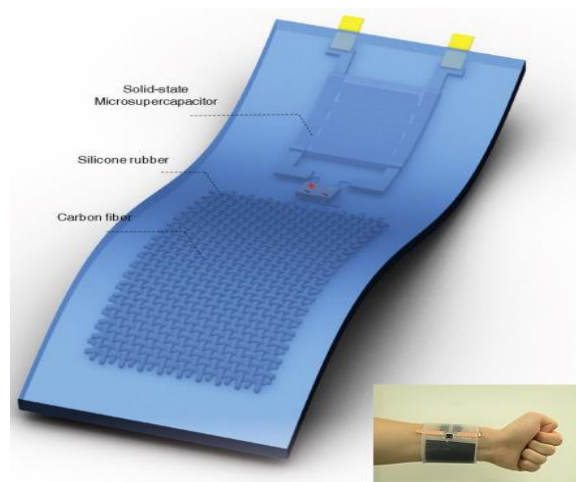
Fig 2. 24: Self powered bracelet to be used for real time pulse measurement[106].

- Li et al. made a breakthrough in the field in 2019 by developing a symbiotic pacemaker. Figure 2.25 [106] depicts this. It was the first time a self-powered pacemaker was used. The triboelectric materials employed in the TENG fabrication were Al foil and PTFE film. The device was implanted in a pig's body, and the results revealed that a voltage of 65 V was produced, and each pulse gave enough energy to produce endocardial pacing.
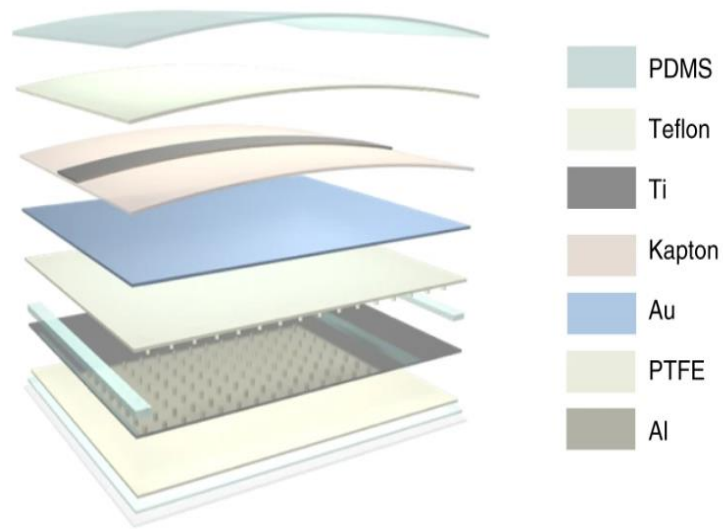
Fig 2. 25: Symbiotic cardiac pacemaker [107].

Chapter 3

Experimental Method

3.1 Synthesis route:

For the synthesis of Bismuth Sodium Titanate nanoparticles, top-down approaches were used. Top-down approaches are discussed in detail below.

3.2 Top-down approach:

3.2.1 Ball Milling Method:

Ball milling is a mechanical process used to grind and mix materials to create a fine powder. The process involves using a rotating drum filled with heavy balls of different sizes as grinding media. As the drum rotates, the balls crush and grind the material to create a fine powder.

The ball milling process can be broken down into several steps:

1. Loading: The materials to be ground are placed into the drum of the ball mill.
2. Grinding: The rotating drum and the balls inside grind the materials into a fine powder.
3. Unloading: Once the grinding is complete, the powder is removed from the drum.

Metals, ceramics, chemicals, and minerals are among the items that can be ground using this method.
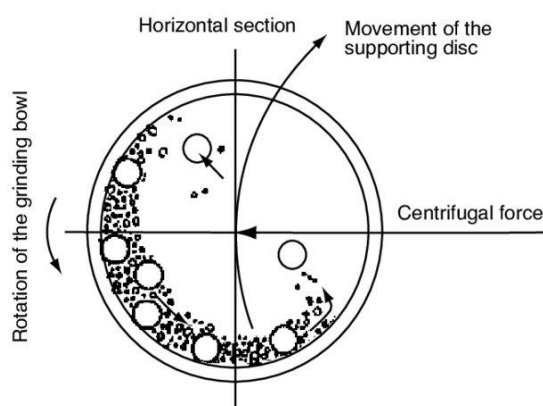
Fig 3. 1: Working principle of ball milling process [108].

Advantages:

- Efficient size reduction
- Controlled particle size and shape
- High throughput
- Low cost

Disadvantages:

- High Energy Consumption
- Risk of Contamination
- Time-Consuming
- Maintenance requirements of the equipment

3.2.2 Laser ablation:

Laser ablation is a physical method used for the synthesis of nanoparticles, which involves the irradiation of a target material by a high-intensity laser pulse. In this process, the laser beam is focused on the surface of the target material, causing its evaporation and ionization. The resulting plasma plume is rapidly quenched, leading to the formation of nanoparticles.
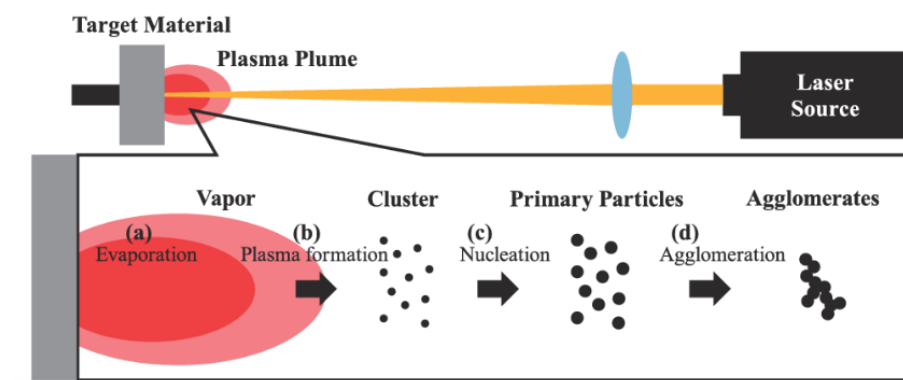
Fig 3. 2: Schematic of particle generation procedure in the laser ablation process [109].

Advantages:

- High purity
- Uniformity
- Control over the nanoparticles' shape and size

38

- Non-contact process
- Laser cutters are CNC devices that are easily automatable and capable of carrying out highly precise operations.

Disadvantages:

- High cost of the laser source
- Difficulty in scaling up the production process
- Lasers are high-energy light beams that can cause severe health and fire concerns.

3.2.3 Electron beam lithography (EBL):

A focussed electron beam is utilized in the nanofabrication process known as electron beam lithography (EBL) to make patterns on a substrate. The substrate can be constructed from a wide range of substances, including silicon, glass, and polymers. The electrons are typically produced by an electron cannon and focussed to a spot size of a few nanometers using a number of electromagnetic lenses.

In EBL, the electron beam is controlled by a computer program that directs the beam to the desired locations on the substrate. The beam can be turned on and off rapidly, allowing the creation of complex patterns with high resolution and accuracy. The pattern is typically created by selectively exposing a resist material on the substrate to the electron beam, which causes a chemical change in the resist.

After the resist is exposed, it is developed to remove the areas that were not exposed to the electron beam. This leaves behind a patterned resist layer on the substrate that can be used for subsequent processing steps such as etching, deposition, or implantation.
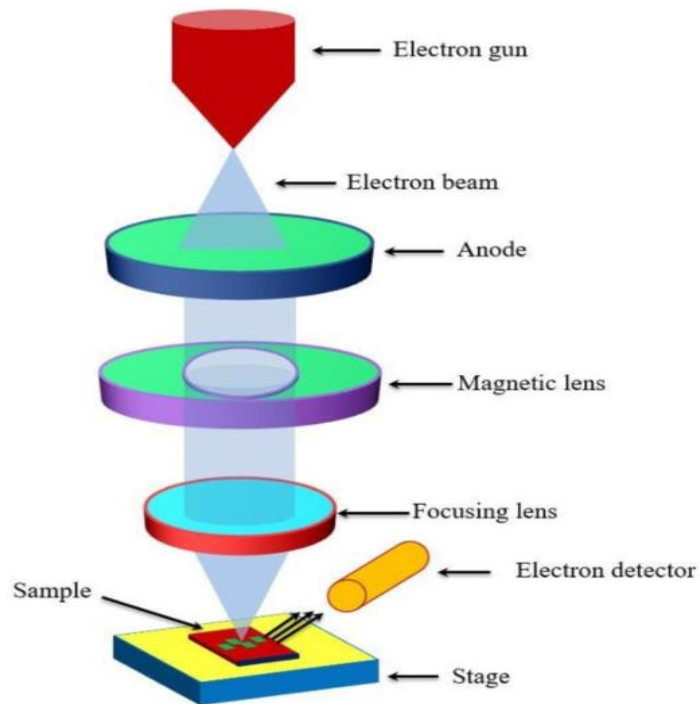
Fig 3. 3: Schematic of Electron beam lithography [110].

Advantages:

- High resolution
- EBL is a flexible technique that can be used to create a wide range of patterns on a variety of substrates. It is also capable of creating complex patterns with high accuracy.
- Direct writing
- No mask required
- Low contamination
- EBL patterns can be easily modified by changing the computer program that controls the electron beam

Disadvantages:

- Slow writing speed
- High cost
- Limited throughput
- Sensitivity to vibrations and environmental factors

- The high-energy electrons used in EBL can cause damage to the resist material and the substrate.

3.2.4 Plasma sputtering:

Plasma sputtering is a thin film deposition process that employs a plasma to create ions that are then directed towards a target material. The procedure is carried out in a vacuum chamber, where a low-pressure gas is ionized to produce plasma. The plasma ions are then propelled towards a target substance, ejecting or sputtering atoms or molecules from the target surface. These sputtered atoms then travel through the plasma to form a thin coating on a substrate.
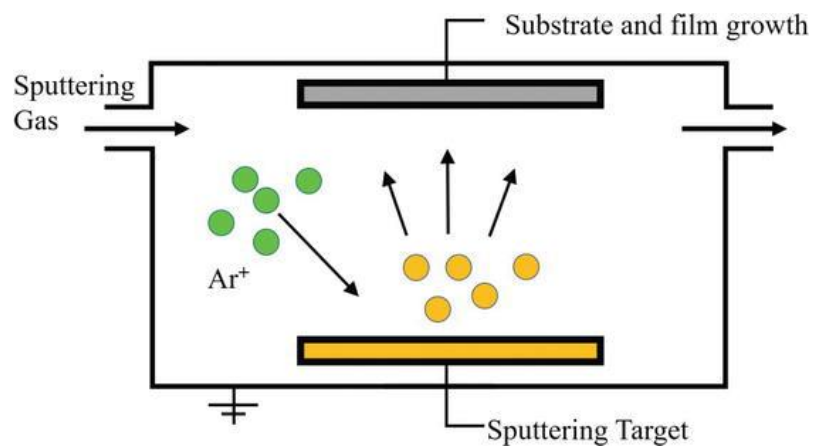
Fig 3. 4: Magnetron sputtering process [111].

Advantages:

- High-quality films

- Versatility

- Low substrate temperature

- High deposition rates

- Minimal waste

- High purity

- Low energy consumption

Disadvantages:

- Equipment cost

- Limited deposition area

- Target material consumption

- Deposition rate limitations

- Film thickness uniformity

- Complex process control

- Surface damage to the target material.

3.2.5   Chemical etching:

Chemical etching is a technique for using chemical processes to remove material from a surface selectively. This process is widely used in the manufacturing of microelectronics, printed circuit boards, metal parts, and other precision components.

The chemical etching process involves the following steps:

1. Cleaning the surface: The surface to be etched is first cleaned to remove any dirt, grease, or other contaminants that may interfere with the etching process.

2. Applying the etchant: The etchant solution is applied to the surface using a spray, dip, or other method. The etchant reacts with the material on the surface and selectively removes it.

3. Monitoring the process: The etching process is monitored closely to ensure that the desired amount of material is removed. This is typically done using visual inspection, chemical analysis, or other methods.

4. Rinsing and drying: Once the desired amount of material has been removed, the surface is rinsed thoroughly with water to remove any remaining etchant. The surface is then dried using a variety of methods, such as air drying, spin drying, or vacuum drying.

Advantages:

- Precision
- Complexity
- Cost-effectiveness
- Versatility
- Minimal material waste
- Consistency
- Speed

Disadvantages:

- Limited thickness
- Surface finish
- Material limitations
- The etchants used in the process can be hazardous to the environment.
- Masking and cleaning requirements
- Equipment limitations

Recently, top-down and bottom-up methods have been designed to fabricate graphene sheets. Top-down methods mainly focus on exfoliation [112].
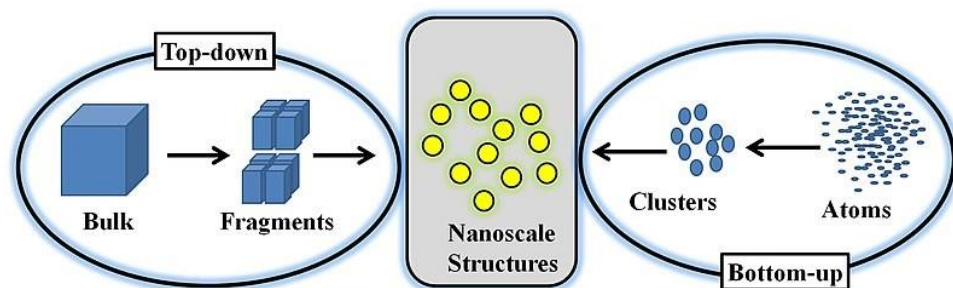
Fig 3. 5: Top-down and bottom-up approach schematic[113].

3.2.6 Exfoliation:

Exfoliation of 2D materials [113] is a hot topic for preparing mono or multilayered materials. Exfoliated materials are significant in terms of both

possible applications and fundamental research. Exfoliated graphite and TMD materials are important because they deliver a breakthrough in flexible electronics and optoelectronics devices. Strong in-plane bonding [114], [115] and weak bonding between layers in 2D materials can be isolated from each other to improve the surface area and potential material characteristics. This process can be done in a variety of ways, including

3.2.6.1   Mechanical Exfoliation:

The layers are separated by mechanical forces in this technique [116] the "scotch tape approach" was used to manufacture graphene from bulk graphite [113]. High quality mono sheets can also be created using this process. This approach is popular because it creates intrinsic sheets, and it is currently the subject of a lot of research.
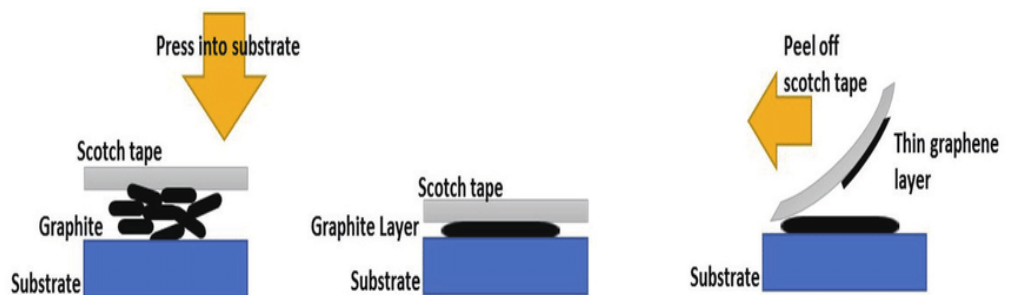
Fig 3. 6: Mechanical Exfoliation of 2D materials [114].

Advantages:

- In most cases, this procedure yields pristine-quality sheets.

Disadvantages

- This technique produces a low yield.
- Lack of scalability in this method [117].
- This approach is unsuitable for mass production.
- Controlling sheet size and thickness is a problem.

3.2.6.2 Liquid Phase Exfoliation:

Solvents are utilized to intercalate the layers of chemicals in this process. Solvents are utilized that have similar surface energy to that of the layered material's crystal lattice. When an appropriate solvent is used in the mixture, sonication forms nanosheets that are stabilized [118]. To achieve well-defined structures, certain surfactants may be applied. For the preparation of mono- and few-layered structures from bulk, sonication assisted exfoliation is currently widely employed. Sound energy is used in sonication, resulting in shear forces. Cavitation bubbles are formed, and as they collapse, the layers are peeled away. The solvent is an important consideration since it must aid in the delimitation process. It should be able to maintain highly stabilized dispersions with a high concentration 2D exfoliated sheets for an extended period. For efficient exfoliation of materials, a mixture of solvents is sometimes used. N-methyl-2-pyrrolidone (NMP) is the most prevalent solvent. The surface energy of NMP is 40 mJ m$_{-2}$, which is similar to that of many-layered materials [119]. n NMP, stable graphite dispersions of up to 40 mg ml-1 with a surface energy of 75 mJ m$_{-2}$ can be achieved.
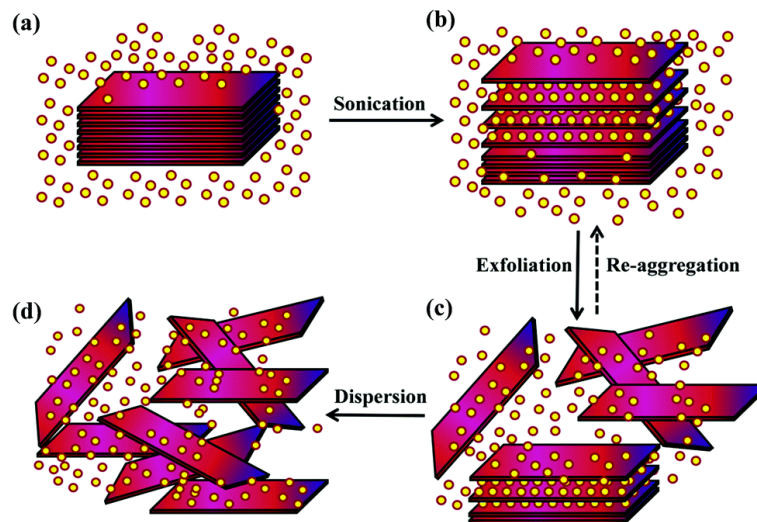
Fig 3. 7: Liquid phase exfoliation of 2D materials [119].

Advantages:

- This method produces a high yield.
- This method is not air sensitive.
- There are no chemical reactions
- The result is a very crystalline product.
- This procedure is extremely straightforward and cost-effective.
- Good scalability sheets are obtained.

Disadvantages:

- The Remaining chemicals in solution-based exfoliation may alter the characteristics of Nanosheets such as graphene. The solvent used could be volatile or toxic.
- This approach can create faults in two-dimensional materials and decrease the flake size to a few hundred nanometers.

3.3 Bottom-up approach:

3.3.1 Sol-gel Method:

The reactants are added together to produce a solution, which is known to be hydrolysis, and later transformed into a gel, which is termed dehydration, afterward drying using thermal treatment, in which the liquid was evaporated from the gel.
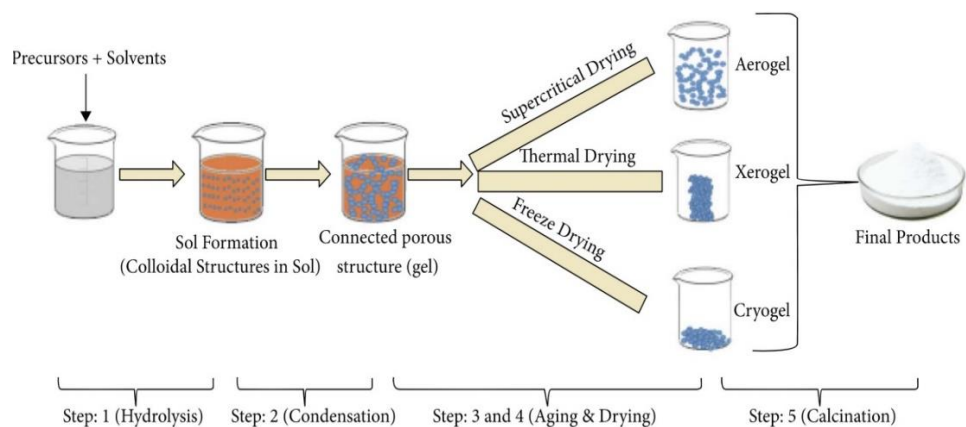
Fig 3. 8: Sol-gel synthesis steps[120].

Advantages:

- It is an easy and affordable method

- High purity

- Good homogeneity

- Low-temperature method

Disadvantages:

- Weak bonding

- Difficult to regulate porosity

3.3.2   Hydrothermal/Solvothermal:

Hydrothermal/solvothermal processes are those in which a reaction takes place in the presence of certain temperature and pressure. For this procedure, a hydrothermal reactor or sealed vessel is utilized, and the precursors are distributed in the solvent and heated to a temperature over their boiling point, resulting in autogenous pressure. The process is known as hydrothermal in the case of water and solvothermal in the case of any other solvent.
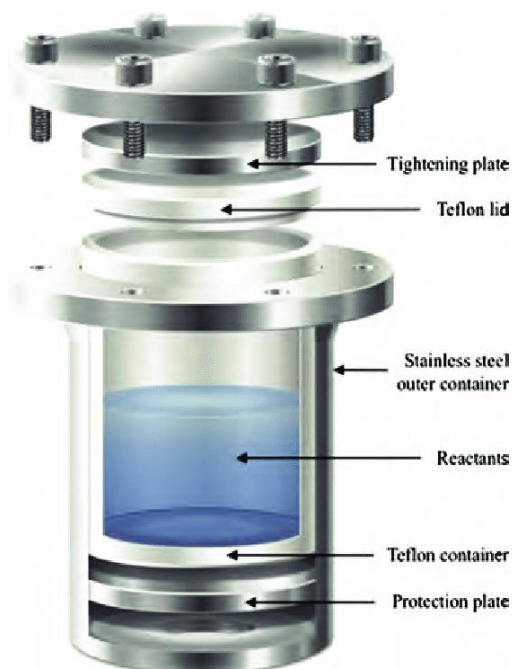
Fig 3. 9: Teflon lined Hydro-thermal reactor [121]

Advantages:

- Simple method

- Changing time, temperature, concentration, and solvent type allows for easy and exact morphology control.

Disadvantages:

- Expensive autoclaves and reactors

- Concerns about safety

3.4 Aim and Objective:

This study aims to synthesize Bismuth Sodium Titanate Nanoparticles to be used with PDMS for Energy harvesting applications. This study includes:

- Synthesis of Bismuth Sodium Titanate Nanoparticles (BNT NPs) through Solid State Method.

- Prepare the composite of the synthesized Bismuth Sodium Titanate NPs with PDMS.

- Synthesis of BNT NPs and PDMS composite film.

- Characterization of the prepared material.

- Fabricating a Hybrid Piezoelectric-Triboelectric Nanogenerator using the composite film

- Testing of the Nanogenerator output using an oscilloscope.

3.5 Choice of Materials:

PDMS is an excellent candidate as it has excellent thermal, elastic, mechanical properties and is environmentally stable. PDMS has a significant ability to gain electrons and stands out due to its flexibility, transparency, and durability [122-128]. To improve the electrical, thermal, and dimensional stability of PDMS, ceramic fillers can be incorporated into it to synthesize a composite. For this purpose, Bismuth Sodium Titanate (BNT) is a good choice of material to be used as the piezoelectric material in the hybrid nanogenerator. BNT is a ferroelectric material, it has a perovskite structure and it can attain four crystal structures according to the temperature. At the temperatures above the Curie point, BNT shows a cubic crystal

system, but at temperatures lower than the Curie point, its structure changes from cubic to tetragonal, with orientation of dipole moment, which results in ferroelectricity in the material [129].

The d_{33} value of BNT synthesized by a solid state reaction is almost 41pC/N [130]. BNT has been found to be a possible energy storage material due to its high spontaneous polarization (P_m) exceeding 40 μC cm^{-2}. The P_m value of BNT is greater than 40 μC cm^{-2} and and hence it is suitable to be used for energy harvesting purpose owing to its high spontaneous polarization [131].

3.6 Selected Synthesis Method:

- For the synthesis of Bismuth Sodium Titanate Nanoparticles, the Solid State method was employed.
- For the preparation of BNT NPs and PDMS composite film, the solution casting method was used.

3.7 Materials Required:

- Bismuth trioxide (Bi2O3)
- Sodium carbonate (Na_2CO_3)
- Titanium dioxide (TiO_2)
- Ethanol
- Zirconia Balls
- Distilled water
- Iso-propanol
- Kapton tape
- Copper Tape
- Copper wires
- Double Sided Tape
- Al foil

3.8 Apparatus used:

- Furnace
- Oven
- Ball mill machine
- Magnetic stirrer
- Hotplate
- Beakers
- Petri dishes
- Weighing balance
- Fume hood

3.9 Synthesis of Bismuth SodiumTitanate Nano-particles:

```
┌─────────────────┐      ┌─────────────────┐
│  Zirconia Balls │      │     Ethanol     │
└─────────────────┘      └─────────────────┘
                  │
                  ▼
         ┌─────────────────┐
         │     Mixing      │
         └─────────────────┘
                  │
                  ▼
         ┌─────────────────┐
         │       Add       │
         │ Na₂CO₃+ TiO₂+ Bi₂O₃ │
         └─────────────────┘
                  │
                  ▼
         ┌─────────────────┐
         │   Ball Milling  │
         └─────────────────┘
                  │
                  ▼
         ┌─────────────────┐
         │    Grinding     │
         └─────────────────┘
                  │
                  ▼
         ┌──────────────────────────┐
         │ Placed powder in furnace │
         └──────────────────────────┘
```

The "Add" box contains: Add $Na_2CO_3 + TiO_2 + Bi_2O_3$
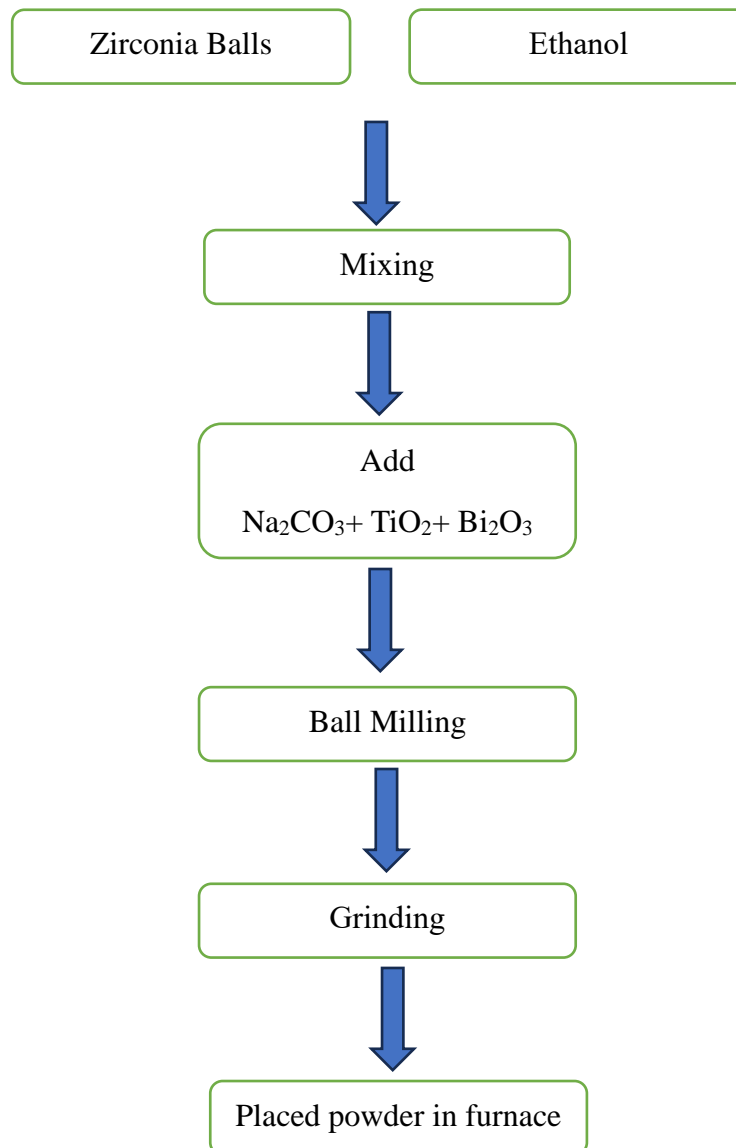
First of all, Zirconia balls and Ethanol were mixed in a breaker. Then 13.0 gram of Bi_2O_3, 2.9 gram of Na_2CO_3 and 8.9 gram of TiO_2 were added to the solution.

The solution was then placed into a Ball mill machine at 220 RPM for 24 hours and then it was put into a drying oven for 12 hours at 90°C. After 12 hours, it was cooled down to room temperature and then grind it in Agate mortar.

After grinding, the powder was placed in furnace for 2 hours at 850°C. After 2 hours, it was cooled down to room temperature and then again grind it in Agate mortar.

3.10 Synthesis of BNT Pallets:
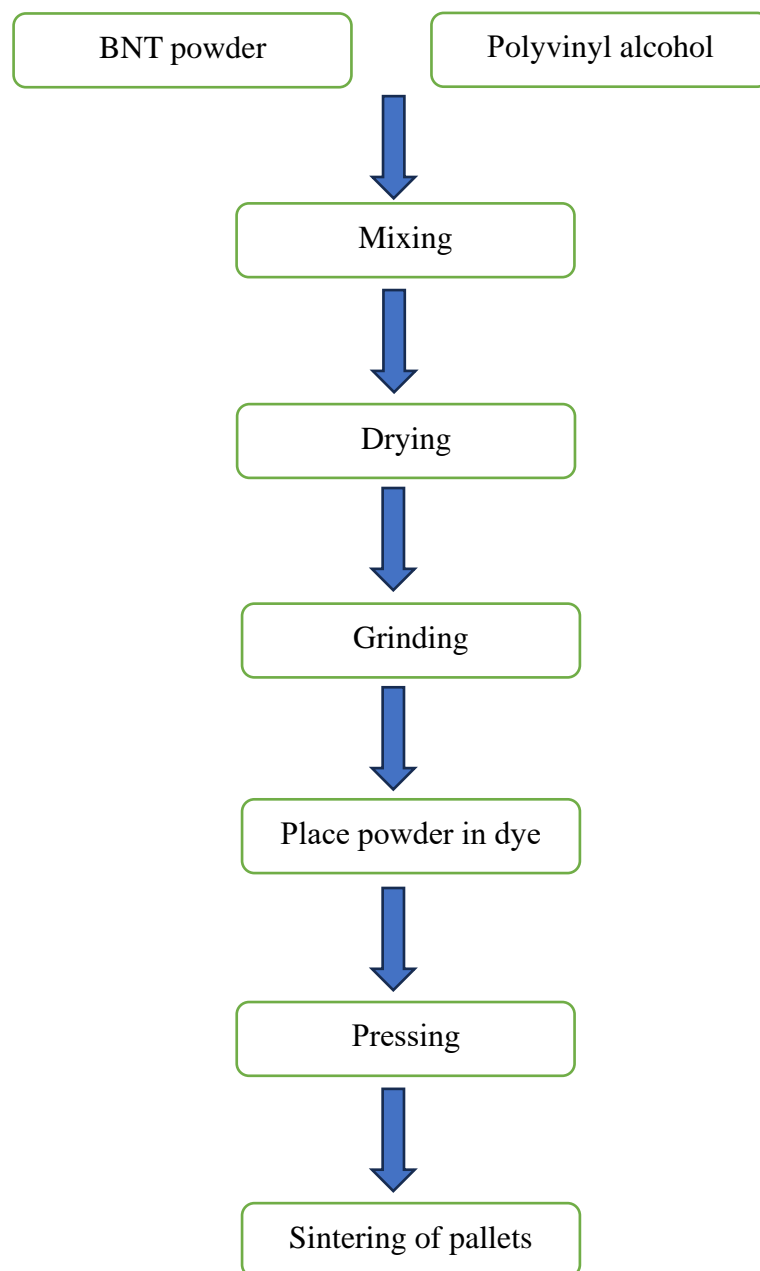
Firstly, 10.0 gram of BNT powder and 20% polyvinyl alcohol were mixed in Agate mortar for 5 min. Then powder was put into a drying oven for 30 minutes at 80°C. The powder was again ground in Agate mortar for 5 minutes. Then 1 gram of powder was placed in dye and pressed with 4-ton pressure.

After pressing, the pallets were formed and sintered these pallets in tube furnace at 550°C to 1150°C for 4 hours.

3.11 Electrode Formation:

First of all, DIM-1005 paste was applied to one side of pallet and placed in drying oven for 30 minutes at 90°C. After that on the other side of the pallet the paste was applied and placed in drying oven for 30 minutes at 90°C.

3.12 Fabrication of BNT-PDMS film:

10 vol % BNT NPs were loaded into PDMS such that the particles were first mixed with Isopropyl alcohol (Isopropanol) by magnetic stirring for 30 mins, and the slurry was then sonicated with an ultrasonication bath for an hour. After sufficient mixing of BNT NPs and Isopropanol, silicone elastomer and its curing agent were added to the solution by a ratio of 10:1. The solution was then left for magnetic stirring for an hour. The film was synthesized by solution casting method by Kapton tape with a regular surface. The sample was left in a drying oven for overnight drying at 90°C, the film was then peeled off the substrate as shown in figure 3.10.
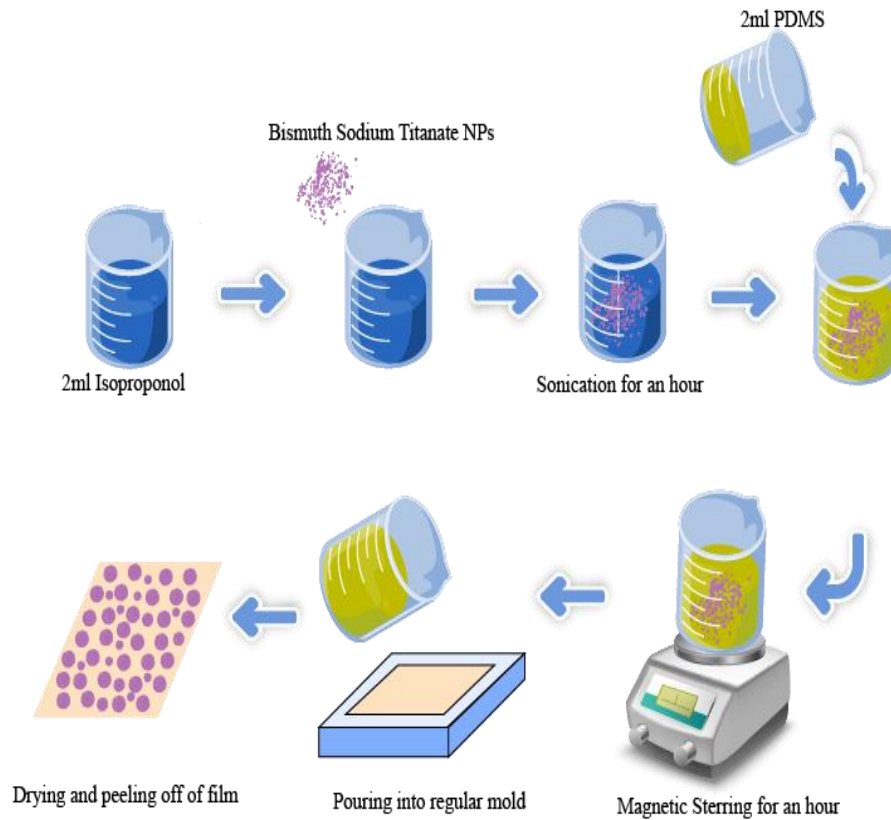
Fig 3. 10: Fabrication Steps of BNT-PDMS Film

3.13 Fabrication of Nanogenerator:

For the fabrication of the Nanogenerator, BNT-PDMS Composite film was used as a tribonegative layer, Al foil served the purpose of the tribo-positive layer as well as the electrode and Cu wires were used to make connections. For this Nanogenerator, contact separation mode was employed by using 4 springs on the corners and Kapton tape was used externally to hold the device and protect the films from the environment.

Fig 3. 11: Picture of the fabricated nanogenerator.

Chapter 4

Characterization Techniques

4.1 Scanning Electron Microscope:

In this technique, the fine beam of electrons is focused over a specimen's surface. As a result, photons or electrons are ejected from the material's surface. The electrons that have been knocked off are then focused on the detector. The detector's output modulates the brightness of the cathode ray tube (CRT). A subsequent point on CRT is plotted for each point where the beams interact, and the material's image is produced [132, 133].

Secondary electrons (SE), backscattered electrons (BSE), and X-rays are produced as a result of the electron-surface interaction [134]. The common SEM mode for detection is via secondary electrons. These electrons are emitted near the surface of the sample. As a result, a distinct and clear image of the sample is obtained. It can disclose sample detail as little as 1nm in size. Elastic scattering of input electrons also occurs, releasing backscattered electrons. In comparison to secondary electrons, they emerge from deeper regions. As a result, their resolution is relatively low. When an inner shell electron is knocked out of its shell, it releases characteristic x-rays [135].

We use SEM because it allows for simple sample preparation and allows us to determine the morphology, chemistry, crystallography, and plane orientation of our samples. SEM magnification can be adjusted from 10 to 500,000 times.

Morphology of the materials was examined on (JEOL-JSM- 6490LA).
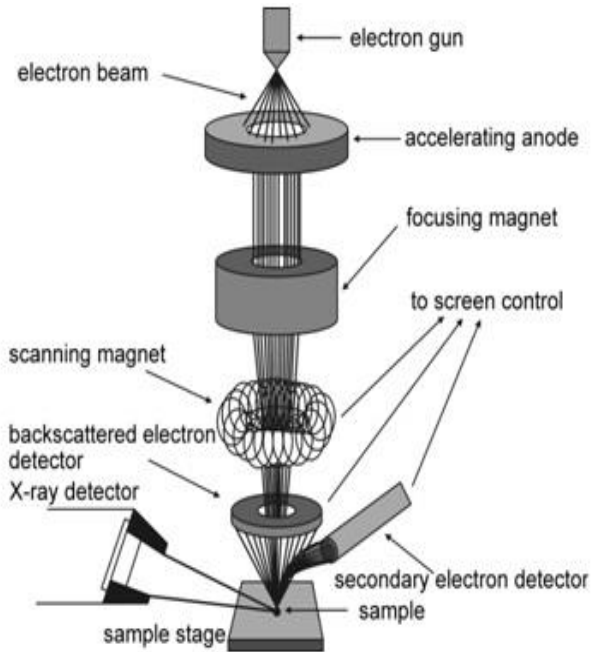
Fig 4. 1: (a) JOEL JSM-6490LA present at SCME; (b) SEM Schematic [123]

4.2   X-Ray Diffraction (XRD):

It is used for the crystal structure determination of the material. It is a non-destructive technique, and it provides fingerprints of Bragg's reflections of crystalline materials. It consists of 3 main parts. A cathode tube, sample holder, and detector. X-rays are produced by heating filament element which accelerates electrons towards a target that collide with target material with electrons. Crystal is composed of layers and planes.

So, an x-ray which has a wavelength similar to these planes is reflected that that angle of incidence is equal to the angle of reflection. "Diffraction" takes place and it can be described as by Bragg's Law:

$$2d\sin\theta = n\lambda \ \text{……. (3)}$$

When Bragg's law is satisfied, it means there is constructive interference, and "Bragg's reflections" will be picked up by the detector. These reflection positions tell us about inter-layer spacing-ray diffraction tells us about the phase, crystallinity, and sample purity. By this technique, one can also determine lattice mismatch, dislocations, and unit cell dimensions. X-ray diffractions were performed by STOE diffractometer at SCME-NUST. The scan angle was taken from 10° to 90°.
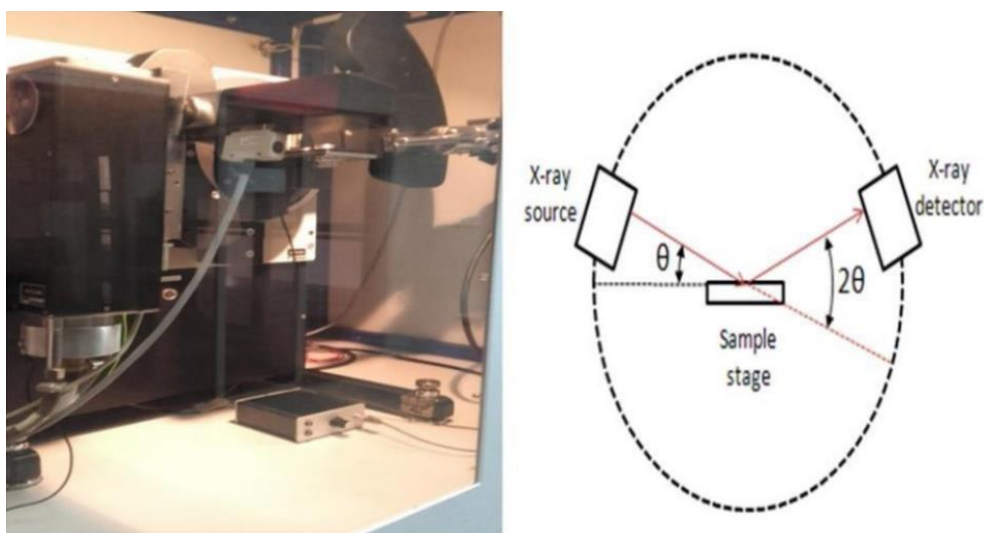
Fig 4. 2: (a) XRD present at SCME- NUST (b) XRD basic schematics

4.3 FTIR:

FTIR spectroscopy works on the principle of Fourier transform. In this, the sample is exposed to a beam of infrared radiation, which causes the molecules in the sample to vibrate. The amount of radiation absorbed by the sample at different frequencies is measured, and the resulting spectrum is analysed to identify the different functional groups present in the sample.

The basic components of an FTIR spectrometer include a source of infrared radiation (usually a Michelson interferometer), a sample holder, a detector, and a computer for data analysis. The Michelson interferometer splits the infrared beam into two paths,

one that passes through the sample and one that does not. The two beams are then recombined, and the resulting interference pattern is recorded by the detector.

The interference pattern contains information about the different frequencies of radiation absorbed by the sample. A Fourier transform is then applied to the interference pattern to generate the infrared spectrum, which provides a unique fingerprint of the sample. The spectrum is then analysed using software to identify the different functional groups present in the sample. Each functional group absorbs infrared radiation at a unique set of frequencies, which allows for accurate identification of the sample.

FTIR spectroscopy is a powerful analytical technique that can be used for a wide range of applications, including identifying unknown substances, quantifying the amount of a particular substance in a sample, and studying chemical reactions.

4.4 RAMAN:

Raman spectroscopy is a method for examining the molecular vibrational vibrations. A molecule may absorb some of the light energy when it interacts with light, which will cause the molecule to vibrate. The Raman effect occurs when the scattered light is shifted in frequency due to the interaction with the molecule's vibrations.

Raman spectroscopy can be used to identify and characterize the chemical composition of materials, determine molecular structure, and study chemical reactions. it can be used to study samples in situ, meaning that the sample does not need to be prepared or altered in any way before analysis. This makes Raman spectroscopy a valuable tool for studying materials in their natural state.

In order to identify the vibrational modes of the sample, a laser beam is focused on the sample, and the scattered light is collected and examined. The intensity of the scattered light is plotted against its frequency shift in relation to the incident laser light to produce the Raman spectrum.

The absorption spectrum of a molecule can provide information about the energy levels and electronic transitions within the molecule. This can be useful in determining the identity of an unknown substance or in studying the properties of complex molecules.

4.5 Digital Oscilloscope:

A digital oscilloscope is used to perform the electronic tests on the sample, it works by plotting graphical results in 2D of the voltages changing with respect to time. It is mostly used to show the waveforms on the display with are else not observed by the human eye as they occur very instantly. The waveforms can be later interpreted to find out about different features such as frequency, amplitude, time interval, etc. Formerly, to find out about these properties, it was required to measure the values using the waveforms that are displayed on the screen, but the recent digital oscilloscopes are capable of directly measuring the values and displaying them on the screen.

Oscilloscopes are used for many applications such as engineering, medicine, and also telecommunication industry. The usual use of this instrument is basically to maintain and check the electronic instruments. There are generally four parts of the analogue oscilloscope that are: vertical controls, horizontal controls, trigger controls, and the display. The display is a cathode ray tube (CRT) and it has vertical and horizontal lines as references. Other than that, the oscilloscopes are also equipped with a probe and the probe is connected to the input on the instrument. For the measurement of the values of current and voltages, the oscilloscope (RIGOL Digital Oscilloscope DS1000E series) was used.

Chapter 5

Results and Discussion

XRD of BNT NPs:

The crystal structure of synthesized BNT powder samples was characterized by an X-ray diffractometer with Cu/Kα radiation. The scanned diffractograms spread over the 2θ values from 20° to 90°, and the scan time was 20 minutes. Diffraction peaks for prepared BNT nanoparticles are observed at 2θ = 22.86°, 32.50°, 40.19°, 46.75°, 52.67°, 58.17°, 68.29°, 77.69°, and these peaks represent the Bragg reflections from the (001), (110), (111), (002), (201), (112), (220) and (113) planes respectively as shown in figure 5.1. The peaks reveal that the crystal structure of the particles is hexagonal and the XRD patterns match precisely with the standard XRD pattern of BNT particles (JCPDS card no. 36-0340). The rhombohedral crystal structure of the particles can also be confirmed from the XRD peak splitting at 2θ~45.
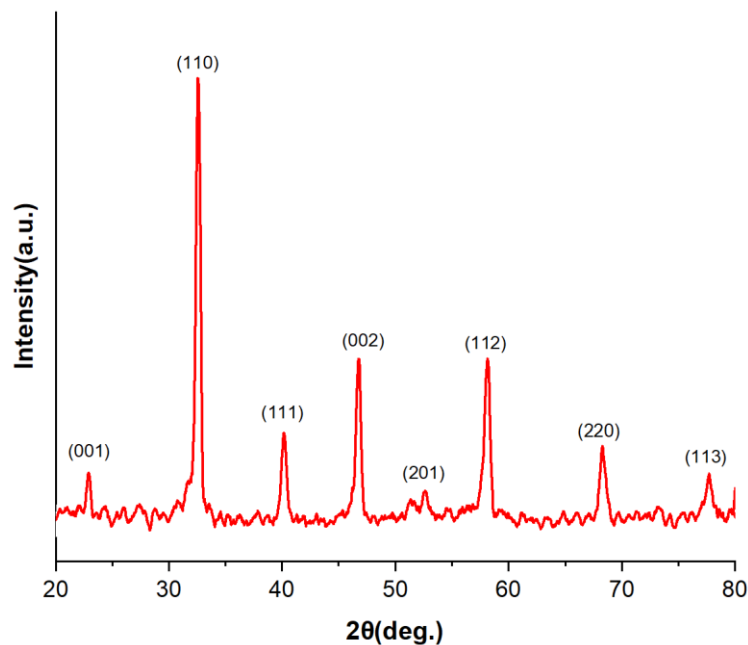
Fig 5. 1: XRD of BNT NPs

SEM of BNT NPs:

The particle size and morphology of BNT ceramics were examined using scanning electron microscopy (SEM), as demonstrated in Figure 5.2 (a, b). The micrographs clearly reveal distinct variations in grain size and shape. On average, the BNT particles exhibit a rounded shape, which can be attributed to the ball milling process conditions. Previous literature reports have also indicated that the ball milling process produces nearly spherical submicron particles.
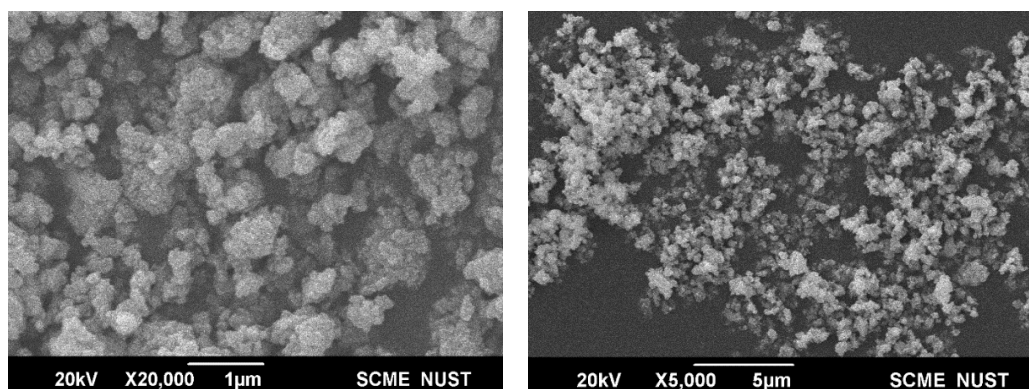
Fig 5. 2: a, b: SEM Images of Bismuth Sodium Titanate particles.

FTIR of BNT NPs:

We examined the infrared Fourier spectra of BNT powders. While O-H's stretching mode is at 3415 cm^{-1}, H-O-H's bending mode appears at 1635 cm^{-1} [136]. he C-H stretching mode is indicated by two peaks at 2854 and 2921 cm^{-1}. The CO vibration is attributed to peaks at 1076 cm^{-1} [137]. Ti-O vibration has been given the range of 650 to 550 cm^{-1} by Music et al [138]. Additionally, characteristic bands at 846.37 cm^{-1} demonstrate the creation of a titanate structure. Ti-O stretching vibrations are considered to be the cause of this band [139].
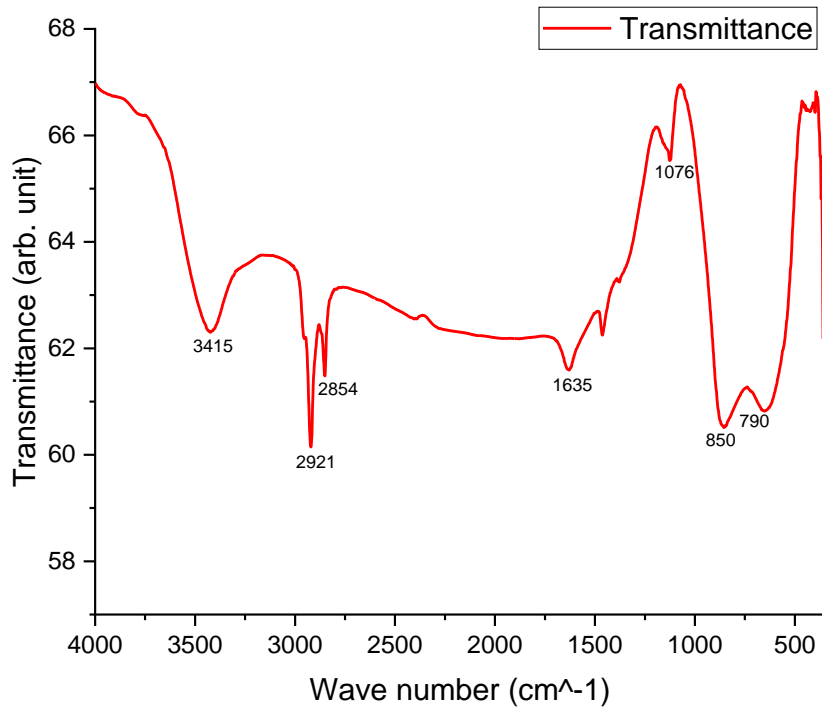
Fig 5. 3: FTIR of BNT NPs

RAMAN of BNT NPs:

BNT's RAMAN spectra were examined. According to Niranjan et al. [140] , Bi ions predominate in the frequency range 109-134 cm^{-1}, while Na-O vibrations predominate in the range 155-187 cm^{-1} [141]. The TiO_6 octahedra's vibrations dominate broad bands between 430 and 670 cm^{-1} [142]. The overlapping A1(LO) and E(LO) bands are responsible for the broad peaks between 700 and 900 cm^{-1}[143].

Based on this study, the I, II, and III sections of the pure $(Na_{0.5}Bi_{0.5})TiO_3$ Raman spectra are designated, as illustrated in Fig. 5.4. Bi-O and Na-O vibrations are correlated with region I, TiO_6 vibrations are correlated with region II, and BNT oxygen vibrations are correlated with region III. The vibrational phonon frequencies of pure NBT and the modes ascribed based on published research are shown in Table 1.
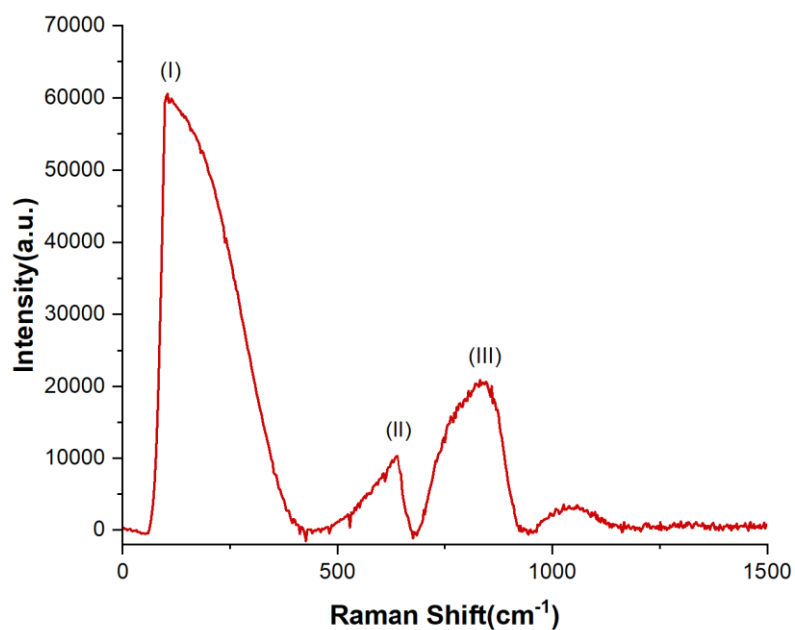
Fig 5. 4: RAMAN of BNT NPs

Table 1: Vibrational phonon frequencies of pure BNT.

S.No	Modes	Theory (cm⁻¹)	Present (cm⁻¹)	Niranjan et al . [140](cm⁻¹)	Suchanicz et al . [144](cm⁻¹)
1	E(TO1)	109	114	-	-
2	A1(TO1)	134	139	141	142
3	A1(LO2)	178	173	-	-
4	E(TO2)	246	252	-	-
5	E(TO8)	549	551	527	531
6	E(LO8)	591	609	-	585
7	A1(LO8)	737	750	750	748
8	A1(LO9)	830	829	869	860

The Working Hybrid Nano-generator:

It is known that using piezoelectric materials in TENG devices could improve their output performance [145, 146], hence in our work 10% vol BNT-NPs were loaded into PDMS and the composite film was rubbed with Al foil as PDMS and Al are far away from each other in the triboelectric series and there would be more charge generation. The composite layer attains a negative charge as it has the tendency to gain electrons and Al foil has the tendency to lose electrons, hence the positive charge. The device won't produce any triboelectric charges in the initial state as there is no friction between the layers yet and there won't be any piezoelectric charges as well, as there is pressure and hence there would be no electrical output at this stage as the electric dipoles generated from the BNT NPs inside the film are balanced at this point, leaving no net charge on the surface. However, when pressure is applied, the surface of layers rubs against each other, and triboelectric charges are generated, the piezoelectric charges are also generated at this point when electric dipoles are unbalanced, due to their stress-induced orientation inside the film, hence net positive and negative charges would be induced on the opposite film surfaces which would lead to the flow of piezoelectric charges. In this case, both phenomena are taking place, leading to increased output. The composite layer would steal electrons from Al foil as it has a stronger affinity for a negative charge, due to this Al foil would attain a positive charge while the composite layer becomes negatively charged. Now the electric polarity has been generated after the pressure is removed and the layers are separated. Due to electrostatic induction, the composite would induce its oppositely generated charges from Al foil to the bottom Al foil, leading to a positive output current when electrons were driven to the top Al foil. As shown in figure 5.5. When the layers are fully separated by the distance of 1 cm, then there would be no charge transfer due to electrical equilibrium. However, the induced charges would reappear when the pressure is applied again.
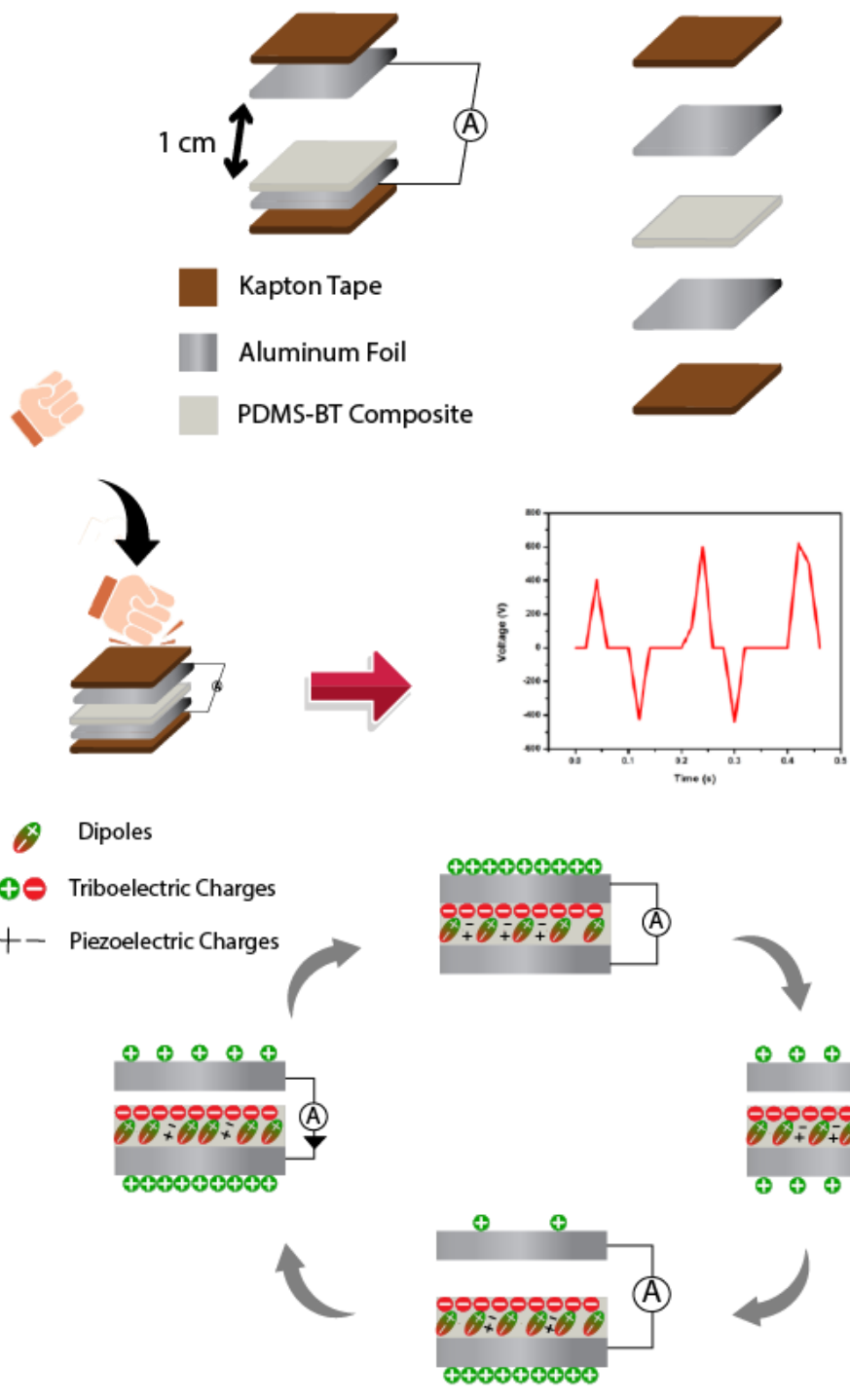
Fig 5. 5: Working Mechanism of Hybrid TENG-PENG Device

Electrical Output performance of devices:

To calculate the output voltage and current of the devices, an oscilloscope of internal resistance 1MΩ was used. To measure the current, a 1MΩ resistor was used externally to obtain current graphs. For the nanogenerator, the contact-separation method was employed to generate the voltage and current, the hand-tapping method was used as the operation condition and both devices had a contact area of 4×4cm2 with the test distance between the two layers of about 1cm. For the contact separation mode, two dissimilar dielectric films are facing each other, and electrodes are attached at the top and bottom of the stacked films, when the films come in contact with each other, it creates oppositely charged surfaces and a potential drop is created as the films are separated. When the films are connected by a load, free electrons flow to balance the electrostatic field, and the potential is dropped again as films come in contact with each other again. The oscilloscope readings revealed that the output voltage of the nanogenerator reached at most about 23V and the output current reached around 46μA.
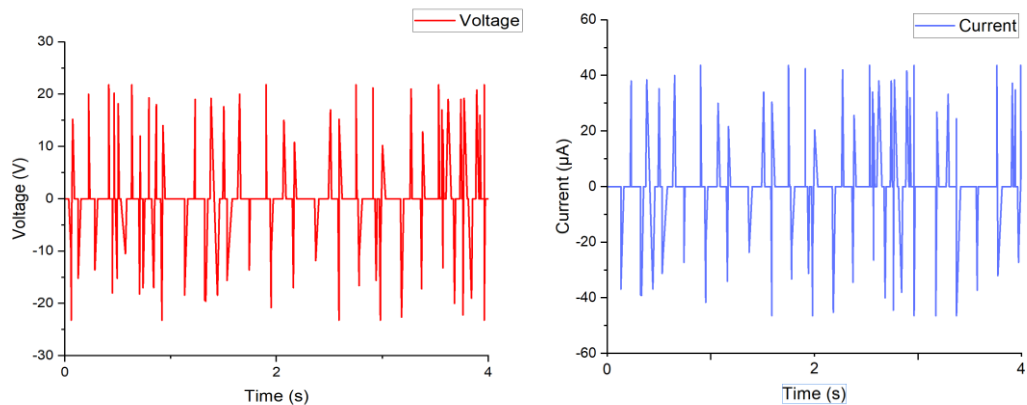
Fig 5. 6: Output Current and Voltage of Hybrid TENG-PENG Device

Some of the recent work done on TENG devices have been mentioned in table 2.

Researchers have used different methods to their material including lithography, chemical treatment, and CO_2 laser ablation as shown and it plays a huge role in enhancing the output performance of the TENG devices.

Table 2: Comparison of recent work done and their output performance

Materials	Fabrication Method	Output Current (μA)	Output Voltage (V)	Ref
ITO/PET-PDMS	Lithography	0.7	18	[20]
Au/PDMS	ICP Etcher	3.2	83	[147]
Al/PDMS	Lithography	8.3	72	[148]
Al/PDMS-BNT	Hand Tapping	46	23	This work

Conclusion:

In summary, a Hybrid Triboelectric and Piezoelectric Nanogenerator was fabricated by using PDMS and Bismuth Sodium Titanate as the primary materials. Bismuth Sodium Titanate Nanoparticles were synthesized by using the Solid-State method and for the characterization of the particles, XRD, SEM, RAMAN and FTIR was performed. The Bismuth Sodium Titanate particles were then utilized to make their composite with PDMS and their film was produced using Kapton Tape Mold and the method for the film casting was simply solution casting. These films were then used with Al foil and Kapton tape to fabricate a Hybrid Triboelectric and Piezoelectric Nanogenerator. For the nanogenerator, PDMS-BNT film was used as a tribonegative material, meanwhile, Al foil was used as a tribopositive layer as well as the electrode and contact separation mode were utilized to couple piezoelectric and triboelectric effects together. The pressing of film, induced dipoles in it due to deformation, meanwhile, the triboelectric charges were formed due to the contact and separation. The capacitance and tangent loss of BNT pallets was tested by the help of impedance analyzer. The electrical performance of the nanogenerator was tested by using a digital oscilloscope. The results of output voltage and current indicated that the surface morphology plays a huge role in enhancing the triboelectric effects.

References

[1]   J. P. Painuly, "Barriers to renewable energy penetration; a framework for analysis," *Renewable energy,* vol. 24, pp. 73-89, (2001).

[2]   N. L. Panwar, S. C. Kaushik, and S. Kothari, "Role of renewable energy sources in environmental protection: A review," *Renewable and sustainable energy reviews,* vol. 15, pp. 1513-1524, (2011).

[3]   S. P. Beeby, R. N. Torah, M. J. Tudor, P. Glynne-Jones, T. O'Donnell, C. R. Saha*, et al.*, "A micro electromagnetic generator for vibration energy harvesting," *Journal of Micromechanics and microengineering,* vol. 17, p. 1257, (2007).

[4]   I. Abed, N. Kacem, N. Bouhaddi, and M. L. Bouazizi, "Multi-modal vibration energy harvesting approach based on nonlinear oscillator arrays under magnetic levitation," *Smart Materials and Structures,* vol. 25, p. 025018, (2016).

[5]   S. P. Beeby, M. J. Tudor, and N. White, "Energy harvesting vibration sources for microsystems applications," *Measurement science and technology,* vol. 17, p. R175, (2006).

[6]   P. D. Mitcheson, P. Miao, B. H. Stark, E. Yeatman, A. Holmes, and T. Green, "MEMS electrostatic micropower generator for low frequency operation," *Sensors and Actuators A: Physical,* vol. 115, pp. 523-529, (2004).

[7]   V. Janicek and M. Husak, "Designing the 3D electrostatic microgenerator," *Journal of Electrostatics,* vol. 71, pp. 214-219, (2013).

[8]   Y. Qin, X. Wang, and Z. L. Wang, "Microfibre–nanowire hybrid structure for energy scavenging," *nature,* vol. 451, pp. 809-813, (2008).

[9]   X. Wang, J. Song, J. Liu, and Z. L. Wang, "Direct-current nanogenerator driven by ultrasonic waves," *Science,* vol. 316, pp. 102-105, (2007).

[10]   Z. L. Wang and J. Song, "Piezoelectric nanogenerators based on zinc oxide nanowire arrays," *Science,* vol. 312, pp. 242-246, (2006).

[11]   S. Xu, B. J. Hansen, and Z. L. Wang, "Piezoelectric-nanowire-enabled power source for driving wireless microelectronics," *Nature communications,* vol. 1, p. 93, (2010).

[12]   S. Xu, Y. Qin, C. Xu, Y. Wei, R. Yang, and Z. L. Wang, "Self-powered nanowire devices," *Nature Nanotechnology,* vol. 5, pp. 366-373, 5/2010 (2010).

[13]   R. Yang, Y. Qin, L. Dai, and Z. L. Wang, "Power generation with laterally packaged piezoelectric fine wires," *Nature nanotechnology,* vol. 4, pp. 34-39, (2009).

[14]   F.-R. Fan, Z.-Q. Tian, and Z. L. Wang, "Flexible triboelectric generator," *Nano energy,* vol. 1, pp. 328-334, (2012).

[15]   X. Wang, S. Niu, Y. Yin, F. Yi, Z. You, and Z. L. Wang, "Triboelectric Nanogenerator Based on Fully Enclosed Rolling Spherical Structure for Harvesting Low-Frequency Water Wave Energy," *Advanced Energy Materials,* vol. 5, p. 1501467, 12/2015 (2015).

[16]   M. Han, X. Zhang, W. Liu, X. Sun, X. Peng, and H. Zhang, "Low-frequency wide-band hybrid energy harvester based on piezoelectric and triboelectric mechanism," *Science China Technological Sciences,* vol. 56, pp. 1835-1841, (2013).

[17]   W.-S. Jung, M.-G. Kang, H. G. Moon, S.-H. Baek, S.-J. Yoon, Z.-L. Wang, *et al.*, "High output piezo/triboelectric hybrid generator," *Scientific reports,* vol. 5, p. 9309, (2015).

[18]   W. Tang, Y. Han, C. B. Han, C. Z. Gao, X. Cao, and Z. L. Wang, "Self-Powered Water Splitting Using Flowing Kinetic Energy," *Advanced Materials,* vol. 27, pp. 272-276, 01/2015 (2015).

[19]   Y. Feng, X. Liang, J. Han, K. Han, T. Jiang, H. Li, *et al.*, "Power management and reaction optimization for a self-powered electrochemical system driven by a triboelectric nanogenerator," *Nano Letters,* vol. 21, pp. 5633-5640, (2021).

[20]   F.-R. Fan, L. Lin, G. Zhu, W. Wu, R. Zhang, and Z. L. Wang, "Transparent triboelectric nanogenerators and self-powered pressure sensors based on micropatterned plastic films," *Nano letters,* vol. 12, pp. 3109-3114, (2012).

[21]   Z. Wen, Q. Shen, and X. Sun, "Nanogenerators for self-powered gas sensing," *Nano-micro letters,* vol. 9, pp. 1-19, (2017).

[22]   Y. Su, X. Wen, G. Zhu, J. Yang, J. Chen, P. Bai, *et al.*, "Hybrid triboelectric nanogenerator for harvesting water wave energy and as a self-powered distress signal emitter," *Nano Energy,* vol. 9, pp. 186-195, (2014).

[23]   Z. H. Lin, G. Zhu, Y. S. Zhou, Y. Yang, P. Bai, J. Chen, *et al.*, "A Self-Powered Triboelectric Nanosensor for Mercury Ion Detection," *Angewandte Chemie International Edition,* vol. 52, pp. 5065-5069, 2013-05-03 (2013).

[24]   Z. Wen, H. Guo, Y. Zi, M.-H. Yeh, X. Wang, J. Deng, *et al.*, "Harvesting Broad Frequency Band Blue Energy by a Triboelectric–Electromagnetic Hybrid Nanogenerator," *ACS Nano,* vol. 10, pp. 6526-6534, 2016-07-26 (2016).

[25]   A. G. Bailey, "The charging of insulator surfaces," *Journal of Electrostatics,* vol. 51-52, pp. 82-90, 05/2001 (2001).

[26]   D. J. Lacks and R. Mohan Sankaran, "Contact electrification of insulating materials," *Journal of Physics D: Applied Physics,* vol. 44, p. 453001, 2011-11-16 (2011).

[27]   F. Galembeck, T. A. L. Burgo, L. B. S. Balestrin, R. F. Gouveia, C. A. Silva, and A. Galembeck, "Friction, tribochemistry and triboelectricity: recent progress and perspectives," *RSC Adv.,* vol. 4, pp. 64280-64298, 2014 (2014).

[28]   L. S. McCarty and G. M. Whitesides, "Electrostatic Charging Due to Separation of Ions at Interfaces: Contact Electrification of Ionic Electrets," *Angewandte Chemie International Edition,* vol. 47, pp. 2188-2207, 2008-03-07 (2008).

[29]   C. P. R. Saunders, "A Review of Thunderstorm Electrification Processes," *Journal of Applied Meteorology,* vol. 32, pp. 642-655, 04/1993 (1993).

[30]   J. F. Kok and N. O. Renno, "Electrostatics in wind-blown sand," *Physical review letters,* vol. 100, p. 014501, (2008).

[31]   C. Krauss, M. Horanyi, and S. Robertson, "Experimental evidence for electrostatic discharging of dust near the surface of Mars," *New Journal of Physics,* vol. 5, p. 70, (2003).

[32]   M. R. James, J. S. Gilbert, and S. J. Lane, "Experimental investigation of volcanic particle aggregation in the absence of a liquid phase," *Journal of Geophysical Research: Solid Earth,* vol. 107, pp. ECV 4-1-ECV 4-13, (2002).

[33]   A. Yu, Y. Zhu, W. Wang, and J. Zhai, "Progress in triboelectric materials: toward high performance and widespread applications," *Advanced Functional Materials,* vol. 29, p. 1900098, (2019).

[34] Y. J. Kim, J. Lee, S. Park, C. Park, C. Park, and H.-J. Choi, "Effect of the relative permittivity of oxides on the performance of triboelectric nanogenerators," *RSC advances,* vol. 7, pp. 49368-49373, (2017).

[35] D. J. Lacks, "The Unpredictability of Electrostatic Charging," *Angewandte Chemie International Edition,* vol. 51, pp. 6822-6823, 2012-07-09 (2012).

[36] H. Alisoy, G. Alisoy, S. Hamamci, and M. Koseoglu, "Combined kinetic charging of particles on the precipitating electrode in a corona field," *Journal of Physics D: Applied Physics,* vol. 37, p. 1459, (2004).

[37] J. Lowell and A. Rose-Innes, "Contact electrification," *Advances in Physics,* vol. 29, pp. 947-1023, (1980).

[38] W. Harper, "The Volta effect as a cause of static electrification," *Proceedings of the Royal Society of London. Series A. Mathematical and Physical Sciences,* vol. 205, pp. 83-103, (1951).

[39] R. Zhang, M. Hummelgård, J. Örtegren, M. Olsen, H. Andersson, Y. Yang*, et al.*, "The triboelectricity of the human body," *Nano Energy,* vol. 86, p. 106041, (2021).

[40] S. Matsusaka, H. Maruyama, T. Matsuyama, and M. Ghadiri, "Triboelectric charging of powders: A review," *Chemical Engineering Science,* vol. 65, pp. 5781-5807, 11/2010 (2010).

[41] T. J. Fabish and C. B. Duke, "Molecular charge states and contact charge exchange in polymers," *Journal of Applied Physics,* vol. 48, pp. 4256-4266, 10/1977 (1977).

[42] A. F. Diaz and J. Guay, "Contact charging of organic materials: Ion vs. electron transfer," *IBM Journal of Research and Development,* vol. 37, pp. 249-260, 3/1993 (1993).

[43] H. Mizes, E. Conwell, and D. Salamida, "Direct observation of ion transfer in contact charging between a metal and a polymer," *Applied physics letters,* vol. 56, pp. 1597-1599, (1990).

[44] L. S. McCarty, A. Winkleman, and G. M. Whitesides, "Ionic Electrets: Electrostatic Charging of Surfaces by Transferring Mobile Ions upon Contact," *Journal of the American Chemical Society,* vol. 129, pp. 4075-4088, 2007-04-01 (2007).

[45] R. Zimmermann, S. Dukhin, and C. Werner, "Electrokinetic Measurements Reveal Interfacial Charge at Polymer Films Caused by Simple Electrolyte Ions," *The Journal of Physical Chemistry B,* vol. 105, pp. 8544-8549, 2001-09-01 (2001).

[46] H. T. Baytekin, B. Baytekin, S. Soh, and B. A. Grzybowski, "Is Water Necessary for Contact Electrification?," *Angewandte Chemie International Edition,* vol. 50, pp. 6766-6770, 2011-07-18 (2011).

[47] W. R. Salaneck, A. Paton, and D. T. Clark, "Double mass transfer during polymer-polymer contacts," *Journal of Applied Physics,* vol. 47, pp. 144-147, 1976-01-01 (1976).

[48] J. Lowell, "The role of material transfer in contact electrification," *Journal of Physics D: Applied Physics,* vol. 10, pp. L233-L235, 1977-12-01 (1977).

[49] S. Wang, L. Lin, and Z. L. Wang, "Nanoscale triboelectric-effect-enabled energy conversion for sustainably powering portable electronics," *Nano letters,* vol. 12, pp. 6339-6346, (2012).

[50] M. Kanik, M. G. Say, B. Daglar, A. F. Yavuz, M. H. Dolas, M. M. El-Ashry*, et al.*, "A Motion- and Sound-Activated, 3D-Printed, Chalcogenide-Based

Triboelectric Nanogenerator," *Advanced Materials,* vol. 27, pp. 2367-2376, 04/2015 (2015).

[51] J. Chen, G. Zhu, W. Yang, Q. Jing, P. Bai, Y. Yang, *et al.*, "Harmonic-Resonator-Based Triboelectric Nanogenerator as a Sustainable Power Source and a Self-Powered Active Vibration Sensor," *Advanced Materials,* vol. 25, pp. 6094-6099, 11/2013 (2013).

[52] C. Li, R. Cao, and X. Zhang, "Breathable materials for triboelectric effect-based wearable electronics," *Applied Sciences,* vol. 8, p. 2485, (2018).

[53] Z. H. Lin, G. Cheng, L. Lin, S. Lee, and Z. L. Wang, "Water–solid surface contact electrification and its use for harvesting liquid-wave energy," *Angewandte Chemie International Edition,* vol. 52, pp. 12545-12549, (2013).

[54] G. Zhu, J. Chen, Y. Liu, P. Bai, Y. S. Zhou, Q. Jing, *et al.*, "Linear-Grating Triboelectric Generator Based on Sliding Electrification," *Nano Letters,* vol. 13, pp. 2282-2289, 2013-05-08 (2013).

[55] C. Zhang, T. Zhou, W. Tang, C. Han, L. Zhang, and Z. L. Wang, "Rotating-Disk-Based Direct-Current Triboelectric Nanogenerator," *Advanced Energy Materials,* vol. 4, p. 1301798, 06/2014 (2014).

[56] L. Lin, S. Wang, Y. Xie, Q. Jing, S. Niu, Y. Hu, *et al.*, "Segmentally Structured Disk Triboelectric Nanogenerator for Harvesting Rotational Mechanical Energy," *Nano Letters,* vol. 13, pp. 2916-2923, 2013-06-12 (2013).

[57] P. Bai, G. Zhu, Y. Liu, J. Chen, Q. Jing, W. Yang, *et al.*, "Cylindrical rotating triboelectric nanogenerator," *ACS nano,* vol. 7, pp. 6361-6366, (2013).

[58] M. Zhang, Y. Jie, X. Cao, J. Bian, T. Li, N. Wang, *et al.*, "Robust design of unearthed single-electrode TENG from three-dimensionally hybridized copper/polydimethylsiloxane film," *Nano Energy,* vol. 30, pp. 155-161, 12/2016 (2016).

[59] H. Zhang, Y. Yang, X. Zhong, Y. Su, Y. Zhou, C. Hu, *et al.*, "Single-Electrode-Based Rotating Triboelectric Nanogenerator for Harvesting Energy from Tires," *ACS Nano,* vol. 8, pp. 680-689, 2014-01-28 (2014).

[60] Z.-H. Lin, G. Cheng, S. Lee, K. C. Pradel, and Z. L. Wang, "Harvesting Water Drop Energy by a Sequential Contact-Electrification and Electrostatic-Induction Process," *Advanced Materials,* vol. 26, pp. 4690-4696, 07/2014 (2014).

[61] R. Hinchet, W. Seung, and S. W. Kim, "Recent progress on flexible triboelectric nanogenerators for selfpowered electronics," *ChemSusChem,* vol. 8, pp. 2327-2344, (2015).

[62] S. Niu, Y. Liu, S. Wang, L. Lin, Y. S. Zhou, Y. Hu, *et al.*, "Theoretical Investigation and Structural Optimization of Single-Electrode Triboelectric Nanogenerators," *Advanced Functional Materials,* vol. 24, pp. 3332-3340, 06/2014 (2014).

[63] S. Wang, Y. Xie, S. Niu, L. Lin, and Z. L. Wang, "Freestanding Triboelectric-Layer-Based Nanogenerators for Harvesting Energy from a Moving Object or Human Motion in Contact and Non-contact Modes," *Advanced Materials,* vol. 26, pp. 2818-2824, 05/2014 (2014).

[64] S. Niu, Y. Liu, X. Chen, S. Wang, Y. S. Zhou, L. Lin, *et al.*, "Theory of freestanding triboelectric-layer-based nanogenerators," *Nano Energy,* vol. 12, pp. 760-774, 03/2015 (2015).

[65] G. Zhu, Y. Su, P. Bai, J. Chen, Q. Jing, W. Yang, *et al.*, "Harvesting Water Wave Energy by Asymmetric Screening of Electrostatic Charges on a

Nanostructured Hydrophobic Thin-Film Surface," *ACS Nano,* vol. 8, pp. 6031-6037, 2014-06-24 (2014).

[66]   Z. Zhao, X. Pu, C. Du, L. Li, C. Jiang, W. Hu*, et al.*, "Freestanding flag-type triboelectric nanogenerator for harvesting high-altitude wind energy from arbitrary directions," *ACS nano,* vol. 10, pp. 1780-1787, (2016).

[67]   S. Niu and Z. L. Wang, "Theoretical systems of triboelectric nanogenerators," *Nano Energy,* vol. 14, pp. 161-192, 05/2015 (2015).

[68]   X. Wang, Z. L. Wang, and Y. Yang, "Hybridized nanogenerator for simultaneously scavenging mechanical and thermal energies by electromagnetic-triboelectric-thermoelectric effects," *Nano Energy,* vol. 26, pp. 164-171, 08/2016 (2016).

[69]   Y. Hu, J. Yang, S. Niu, W. Wu, and Z. L. Wang, "Hybridizing triboelectrification and electromagnetic induction effects for high-efficient mechanical energy harvesting," *ACS nano,* vol. 8, pp. 7442-7450, (2014).

[70]   H. Zhang, Y. Yang, Y. Su, J. Chen, C. Hu, Z. Wu*, et al.*, "Triboelectric nanogenerator as self-powered active sensors for detecting liquid/gaseous water/ethanol," *Nano Energy,* vol. 2, pp. 693-701, 09/2013 (2013).

[71]   Q. Liang, X. Yan, Y. Gu, K. Zhang, M. Liang, S. Lu*, et al.*, "Highly transparent triboelectric nanogenerator for harvesting water-related energy reinforced by antireflection coating," *Scientific reports,* vol. 5, p. 9080, (2015).

[72]   C. Yao, A. Hernandez, Y. Yu, Z. Cai, and X. Wang, "Triboelectric nanogenerators and power-boards from cellulose nanofibrils and recycled materials," *Nano Energy,* vol. 30, pp. 103-108, 12/2016 (2016).

[73]   X. Cheng, B. Meng, X. Chen, M. Han, H. Chen, Z. Su*, et al.*, "Single-step fluorocarbon plasma treatment-induced wrinkle structure for high-performance triboelectric nanogenerator," *Small,* vol. 12, pp. 229-236, (2016).

[74]   S. Wang, Y. Xie, S. Niu, L. Lin, C. Liu, Y. S. Zhou*, et al.*, "Maximum Surface Charge Density for Triboelectric Nanogenerators Achieved by Ionized-Air Injection: Methodology and Theoretical Understanding," *Advanced Materials,* vol. 26, pp. 6720-6728, 10/2014 (2014).

[75]   W. Tang, C. Zhang, C. B. Han, and Z. L. Wang, "Enhancing Output Power of Cylindrical Triboelectric Nanogenerators by Segmentation Design and Multilayer Integration," *Advanced Functional Materials,* vol. 24, pp. 6684-6690, 11/2014 (2014).

[76]   W. Wang, J. Pang, J. Su, F. Li, Q. Li, X. Wang*, et al.*, "Applications of nanogenerators for biomedical engineering and healthcare systems," *InfoMat,* vol. 4, p. e12262, (2022).

[77]   X.-S. Zhang, M.-D. Han, R.-X. Wang, F.-Y. Zhu, Z.-H. Li, W. Wang*, et al.*, "Frequency-multiplication high-output triboelectric nanogenerator for sustainably powering biomedical microsystems," *Nano letters,* vol. 13, pp. 1168-1172, (2013).

[78]   B. Meng, W. Tang, Z.-h. Too, X. Zhang, M. Han, W. Liu*, et al.*, "A transparent single-friction-surface triboelectric generator and self-powered touch sensor," *Energy & Environmental Science,* vol. 6, pp. 3235-3240, (2013).

[79]   X. Wang, Y. Gu, Z. Xiong, Z. Cui, and T. Zhang, "Silk-Molded Flexible, Ultrasensitive, and Highly Stable Electronic Skin for Monitoring Human Physiological Signals," *Advanced Materials,* vol. 26, pp. 1336-1342, 03/2014 (2014).

[80] Q. Lu, H. Chen, Y. Zeng, J. Xue, X. Cao, N. Wang, *et al.*, "Intelligent facemask based on triboelectric nanogenerator for respiratory monitoring," *Nano Energy,* vol. 91, p. 106612, (2022).

[81] Z. Zhao, C. Yan, Z. Liu, X. Fu, L. M. Peng, Y. Hu, *et al.*, "Machine-washable textile triboelectric nanogenerators for effective human respiratory monitoring through loom weaving of metallic yarns," *Advanced Materials,* vol. 28, pp. 10267-10274, (2016).

[82] W. Yang, J. Chen, X. Wen, Q. Jing, J. Yang, Y. Su, *et al.*, "Triboelectrification Based Motion Sensor for Human-Machine Interfacing," *ACS Applied Materials & Interfaces,* vol. 6, pp. 7479-7484, 2014-05-28 (2014).

[83] P. Bai, G. Zhu, Q. Jing, J. Yang, J. Chen, Y. Su, *et al.*, "Membrane-Based Self-Powered Triboelectric Sensors for Pressure Change Detection and Its Uses in Security Surveillance and Healthcare Monitoring," *Advanced Functional Materials,* vol. 24, pp. 5807-5813, 10/2014 (2014).

[84] Y. Ma, Q. Zheng, Y. Liu, B. Shi, X. Xue, W. Ji, *et al.*, "Self-powered, one-stop, and multifunctional implantable triboelectric active sensor for real-time biomedical monitoring," *Nano letters,* vol. 16, pp. 6042-6051, (2016).

[85] P.-K. Yang, L. Lin, F. Yi, X. Li, K. C. Pradel, Y. Zi, *et al.*, "A Flexible, Stretchable and Shape-Adaptive Approach for Versatile Energy Conversion and Self-Powered Biomedical Monitoring," *Advanced Materials,* vol. 27, pp. 3817-3824, 07/2015 (2015).

[86] J. H. Kim, W. S. Chang, H. H. Jung, and J. W. Chang, "Effect of Subthalamic Deep Brain Stimulation on Levodopa-Induced Dyskinesia in Parkinson's Disease," *Yonsei Medical Journal,* vol. 56, p. 1316, 2015 (2015).

[87] Q. Zheng, H. Zhang, B. Shi, X. Xue, Z. Liu, Y. Jin, *et al.*, "*In Vivo* Self-Powered Wireless Cardiac Monitoring *via* Implantable Triboelectric Nanogenerator," *ACS Nano,* vol. 10, pp. 6510-6518, 2016-07-26 (2016).

[88] F. Yi, X. Wang, S. Niu, S. Li, Y. Yin, K. Dai, *et al.*, "A highly shape-adaptive, stretchable design based on conductive liquid for energy harvesting and self-powered biomechanical monitoring," *Science advances,* vol. 2, p. e1501624, (2016).

[89] Y. C. Lai, J. Deng, S. Niu, W. Peng, C. Wu, R. Liu, *et al.*, "Electric eel-skin-inspired mechanically durable and super-stretchable nanogenerator for deformable power source and fully autonomous conformable electronic-skin applications," *Advanced Materials,* vol. 28, pp. 10024-10032, (2016).

[90] Y.-C. Lai, J. Deng, R. Liu, Y.-C. Hsiao, S. L. Zhang, W. Peng, *et al.*, "Actively Perceiving and Responsive Soft Robots Enabled by Self-Powered, Highly Extensible, and Highly Sensitive Triboelectric Proximity- and Pressure-Sensing Skins," *Advanced Materials,* vol. 30, p. 1801114, 07/2018 (2018).

[91] M. Shi, H. Wu, J. Zhang, M. Han, B. Meng, and H. Zhang, "Self-powered wireless smart patch for healthcare monitoring," *Nano Energy,* vol. 32, pp. 479-487, 02/2017 (2017).

[92] X. Chen, Y. Wu, J. Shao, T. Jiang, A. Yu, L. Xu, *et al.*, "On-skin triboelectric nanogenerator and self-powered sensor with ultrathin thickness and high stretchability," *Small,* vol. 13, p. 1702929, (2017).

[93] K. Dong, J. Deng, Y. Zi, Y.-C. Wang, C. Xu, H. Zou, *et al.*, "3D Orthogonal Woven Triboelectric Nanogenerator for Effective Biomechanical Energy Harvesting and as Self-Powered Active Motion Sensors," *Advanced Materials,* vol. 29, p. 1702648, 10/2017 (2017).

[94]   J. Deng, X. Kuang, R. Liu, W. Ding, A. C. Wang, Y. C. Lai, *et al.*, "Vitrimer elastomer-based jigsaw puzzle-like healable triboelectric nanogenerator for self-powered wearable electronics," *Advanced Materials,* vol. 30, p. 1705918, (2018).

[95]   K. Meng, J. Chen, X. Li, Y. Wu, W. Fan, Z. Zhou, *et al.*, "Flexible weaving constructed self-powered pressure sensor enabling continuous diagnosis of cardiovascular disease and measurement of cuffless blood pressure," *Advanced Functional Materials,* vol. 29, p. 1806388, (2019).

[96]   Z. Liu, Y. Ma, H. Ouyang, B. Shi, N. Li, D. Jiang, *et al.*, "Transcatheter Self-Powered Ultrasensitive Endocardial Pressure Sensor," *Advanced Functional Materials,* vol. 29, p. 1807560, 01/2019 (2019).

[97]   W.-J. Lai, C.-W. Hsueh, and J.-L. Wu, "A fully decentralized time-lock encryption system on blockchain," in *2019 IEEE International Conference on Blockchain (Blockchain)*, (2019), pp. 302-307.

[98]   G. Yao, L. Xu, X. Cheng, Y. Li, X. Huang, W. Guo, *et al.*, "Bioinspired triboelectric nanogenerators as self-powered electronic skin for robotic tactile sensing," *Advanced Functional Materials,* vol. 30, p. 1907312, (2020).

[99]   Z. Lin, J. Yang, X. Li, Y. Wu, W. Wei, J. Liu, *et al.*, "Large-scale and washable smart textiles based on triboelectric nanogenerator arrays for self-powered sleeping monitoring," *Advanced Functional Materials,* vol. 28, p. 1704112, (2018).

[100]   T.-C. Hou, Y. Yang, H. Zhang, J. Chen, L.-J. Chen, and Z. Lin Wang, "Triboelectric nanogenerator built inside shoe insole for harvesting walking energy," *Nano Energy,* vol. 2, pp. 856-862, 09/2013 (2013).

[101]   W. Yang, J. Chen, G. Zhu, J. Yang, P. Bai, Y. Su, *et al.*, "Harvesting Energy from the Natural Vibration of Human Walking," *ACS Nano,* vol. 7, pp. 11317-11324, 2013-12-23 (2013).

[102]   Q. Zheng, Y. Zou, Y. Zhang, Z. Liu, B. Shi, X. Wang, *et al.*, "Biodegradable triboelectric nanogenerator as a life-time designed implantable power source," *Science advances,* vol. 2, p. e1501478, (2016).

[103]   P. Song, S. Kuang, N. Panwar, G. Yang, D. J. H. Tng, S. C. Tjin, *et al.*, "A Self-Powered Implantable Drug-Delivery System Using Biokinetic Energy," *Advanced Materials,* vol. 29, p. 1605668, 03/2017 (2017).

[104]   Z. Lin, J. Chen, X. Li, Z. Zhou, K. Meng, W. Wei, *et al.*, "Triboelectric Nanogenerator Enabled Body Sensor Network for Self-Powered Human Heart-Rate Monitoring," *ACS Nano,* vol. 11, pp. 8830-8837, 2017-09-26 (2017).

[105]   Q. Jiang, C. Wu, Z. Wang, A. C. Wang, J.-H. He, Z. L. Wang, *et al.*, "MXene electrochemical microsupercapacitor integrated with triboelectric nanogenerator as a wearable self-charging power unit," *Nano Energy,* vol. 45, pp. 266-272, (2018).

[106]   H. Ouyang, Z. Liu, N. Li, B. Shi, Y. Zou, F. Xie, *et al.*, "Symbiotic cardiac pacemaker," *Nature Communications,* vol. 10, p. 1821, 2019-04-23 (2019).

[107]   P. Jittiarporn, S. Badilescu, M. N. Al Sawafta, L. Sikong, and V.-V. Truong, "Electrochromic properties of sol–gel prepared hybrid transition metal oxides – A short review," *Journal of Science: Advanced Materials and Devices,* vol. 2, pp. 286-300, 09/2017 (2017).

[108]   C. Suryanarayana, "Mechanical alloying and milling," *Progress in materials science,* vol. 46, pp. 1-184, (2001).

[109] M. Kim, S. Osone, T. Kim, H. Higashi, and T. Seto, "Synthesis of nanoparticles by laser ablation: A review," *KONA Powder and Particle Journal,* vol. 34, pp. 80-90, (2017).

[110] P. K. Ghosh, *Study of Plasmonic Properties of the Gold Nanorods in the Visible to Near Infrared Light Regime*: University of Arkansas, (2016).

[111] F. Shi, "Introductory chapter: basic theory of magnetron sputtering," in *Magnetron Sputtering*, ed: IntechOpen, (2018).

[112] A. P. S. Gaur, S. Sahoo, M. Ahmadi, S. P. Dash, M. J.-F. Guinel, and R. S. Katiyar, "Surface Energy Engineering for Tunable Wettability through Controlled Synthesis of MoS $_2$," *Nano Letters,* vol. 14, pp. 4314-4321, 2014-08-13 (2014).

[113] H. Li, J. Wu, Z. Yin, and H. Zhang, "Preparation and Applications of Mechanically Exfoliated Single-Layer and Multilayer MoS $_2$ and WSe $_2$ Nanosheets," *Accounts of Chemical Research,* vol. 47, pp. 1067-1075, 2014-04-15 (2014).

[114] M. Chhowalla, H. S. Shin, G. Eda, L.-J. Li, K. P. Loh, and H. Zhang, "The chemistry of two-dimensional layered transition metal dichalcogenide nanosheets," *Nature Chemistry,* vol. 5, pp. 263-275, 4/2013 (2013).

[115] T. Matsunaga, R. Tomoda, T. Nakajima, and H. Wake, "Photoelectrochemical sterilization of microbial cells by semiconductor powders," *FEMS Microbiology Letters,* vol. 29, pp. 211-214, 08/1985 (1985).

[116] H. Li, Z. Yin, Q. He, H. Li, X. Huang, G. Lu*, et al.*, "Fabrication of Single- and Multilayer MoS2 Film-Based Field-Effect Transistors for Sensing NO at Room Temperature," *Small,* vol. 8, pp. 63-67, 2012-01-09 (2012).

[117] J. Shen, Y. He, J. Wu, C. Gao, K. Keyshar, X. Zhang*, et al.*, "Liquid phase exfoliation of two-dimensional materials by directly probing and matching surface tension components," *Nano letters,* vol. 15, pp. 5449-5454, (2015).

[118] A. Gupta, V. Arunachalam, and S. Vasudevan, "Water dispersible, positively and negatively charged MoS2 nanosheets: surface chemistry and the role of surfactant binding," *The journal of physical chemistry letters,* vol. 6, pp. 739-744, (2015).

[119] G. Cunningham, M. Lotya, C. S. Cucinotta, S. Sanvito, S. D. Bergin, R. Menzel*, et al.*, "Solvent Exfoliation of Transition Metal Dichalcogenides: Dispersibility of Exfoliated Nanosheets Varies Only Weakly between Compounds," *ACS Nano,* vol. 6, pp. 3468-3480, 2012-04-24 (2012).

[120] D. Bokov, A. Turki Jalil, S. Chupradit, W. Suksatan, M. Javed Ansari, I. H. Shewael*, et al.*, "Nanomaterial by sol-gel method: synthesis and application," *Advances in Materials Science and Engineering,* vol. 2021, pp. 1-21, (2021).

[121] Q. Yang, Z. Lu, J. Liu, X. Lei, Z. Chang, L. Luo*, et al.*, "Metal oxide and hydroxide nanoarrays: Hydrothermal synthesis and applications as supercapacitors and nanocatalysts," *Progress in Natural Science: Materials International,* vol. 23, pp. 351-366, 08/2013 (2013).

[122] L. K. Anlin, K. Vijoy, K. Pradeesh, S. Thomas, H. John, and K. Saji, "Effects of metal nanoparticles on the performance of PDMS based triboelectric nanogenerators," *Physica B: Condensed Matter,* vol. 639, p. 413952, (2022).

[123] Y. Liu, E. Li, Y. Yan, Z. Lin, Q. Chen, X. Wang*, et al.*, "A one-structure-layer PDMS/Mxenes based stretchable triboelectric nanogenerator for simultaneously harvesting mechanical and light energy," *Nano Energy,* vol. 86, p. 106118, 08/2021 (2021).

[124] G. Jian, Q. Meng, Y. Jiao, L. Feng, H. Shao, F. Wang, *et al.*, "Hybrid PDMS-TiO2-stainless steel textiles for triboelectric nanogenerators," *Chemical Engineering Journal,* vol. 417, p. 127974, 08/2021 (2021).

[125] C. Chung and K. Ke, "High contact surface area enhanced Al/PDMS triboelectric nanogenerator using novel overlapped microneedle arrays and its application to lighting and self-powered devices," *Applied Surface Science,* vol. 508, p. 145310, (2020).

[126] S. Sriphan, C. Nawanil, and N. Vittayakorn, "Influence of dispersed phase morphology on electrical and fatigue properties of BaTiO3/PDMS nanogenerator," *Ceramics International,* vol. 44, pp. S38-S42, 11/2018 (2018).

[127] B. Dudem, N. D. Huynh, W. Kim, D. H. Kim, H. J. Hwang, D. Choi, *et al.*, "Nanopillar-array architectured PDMS-based triboelectric nanogenerator integrated with a windmill model for effective wind energy harvesting," *Nano Energy,* vol. 42, pp. 269-281, 12/2017 (2017).

[128] K. V. Vijoy, H. John, and K. J. Saji, "Self-powered ultra-sensitive millijoule impact sensor using room temperature cured PDMS based triboelectric nanogenerator," *Microelectronic Engineering,* vol. 251, p. 111664, 01/2022 (2022).

[129] Y. Zhang, G. Liang, S. Tang, B. Peng, Q. Zhang, L. Liu, *et al.*, "Phase-transition induced optimization of electrostrain, electrocaloric refrigeration and energy storage of LiNbO3 doped BNT-BT ceramics," *Ceramics International,* vol. 46, pp. 1343-1351, (2020).

[130] B. Parija, T. Badapanda, V. Senthil, S. Rout, and S. Panigrahi, "Diffuse phase transition, piezoelectric and optical study of Bi 0· 5 Na 0· 5 TiO 3 ceramic," *Bulletin of Materials Science,* vol. 35, pp. 197-202, (2012).

[131] P. Jaita, K. Saenkam, and G. Rujijanagul, "Improvements in piezoelectric and energy harvesting properties with a slight change in depolarization temperature in modified BNKT ceramics by a simple technique," *RSC advances,* vol. 13, pp. 3743-3758, (2023).

[132] K. D. Vernon-Parry, "Scanning electron microscopy: an introduction," *III-Vs review,* vol. 13, pp. 40-44, (2000).

[133] M. Abd Mutalib, M. Rahman, M. Othman, A. Ismail, and J. Jaafar, "Scanning electron microscopy (SEM) and energy-dispersive X-ray (EDX) spectroscopy," in *Membrane characterization*, ed: Elsevier, (2017), pp. 161-179.

[134] D. C. Joy and J. B. Pawley, "High-resolution scanning electron microscopy," *Ultramicroscopy,* vol. 47, pp. 80-100, (1992).

[135] L. Laperrière and G. Reinhart, *CIRP encyclopedia of production engineering*: Springer Berlin, (2014).

[136] C. Y. Kim, T. Sekino, and K. Niihara, "Synthesis of bismuth sodium titanate nanosized powders by solution/sol–gel process," *Journal of the American Ceramic Society,* vol. 86, pp. 1464-1467, (2003).

[137] R. Urlaub, U. Posset, and R. Thull, "FT-IR spectroscopic investigations on sol–gel-derived coatings from acid-modified titanium alkoxides," *Journal of non-crystalline solids,* vol. 265, pp. 276-284, (2000).

[138] S. Musić, M. Gotić, M. Ivanda, S. Popović, A. Turković, R. Trojko, *et al.*, "Chemical and micro structural properties of TiO2 synthesized by sol-gel procedure," *Materials Science and Engineering: B,* vol. 47, pp. 33-40, 1997.

[139] S. Supriya, A. J. Dos santos-García, C. You, and F. Fernández-Martinez, "Analysis of single and binary phases in cerium doped sodium bismuth

titanate-Na0. 5Bi0. 5TiO3 materials," *Energy Procedia,* vol. 84, pp. 190-196, (2015).

[140] M. K. Niranjan, T. Karthik, S. Asthana, J. Pan, and U. V. Waghmare, "Theoretical and experimental investigation of Raman modes, ferroelectric and dielectric properties of relaxor Na0. 5Bi0. 5TiO3," *Journal of Applied Physics,* vol. 113, (2013).

[141] D. J. Ruth and B. Sundarakannan, "Structural and Raman spectroscopic studies of poled lead-free piezoelectric sodium bismuth titanate ceramics," *Ceramics International,* vol. 42, pp. 4775-4778, (2016).

[142] D. Rout, K.-S. Moon, S.-J. L. Kang, and I. Kim, "Dielectric and Raman scattering studies of phase transitions in the (100− x) Na0. 5Bi0. 5TiO3– xSrTiO3 system," *Journal of applied physics,* vol. 108, (2010).

[143] J. Wang, Z. Zhou, and J. Xue, "Phase transition, ferroelectric behaviors and domain structures of (Na1/2Bi1/2) 1− xTiPbxO3 thin films," *Acta materialia,* vol. 54, pp. 1691-1698, (2006).

[144] J. Suchanicz, I. Jankowska-Sumara, and T. V. Kruzina, "Raman and infrared spectroscopy of Na 0.5 Bi 0.5 TiO 3-BaTiO 3 ceramics," *Journal of electroceramics,* vol. 27, pp. 45-50, (2011).

[145] J. Yu, X. Hou, M. Cui, S. Zhang, J. He, W. Geng*, et al.*, "Highly skin-conformal wearable tactile sensor based on piezoelectric-enhanced triboelectric nanogenerator," *Nano Energy,* vol. 64, p. 103923, (2019).

[146] M. Zhu, Q. Shi, T. He, Z. Yi, Y. Ma, B. Yang*, et al.*, "Self-powered and self-functional cotton sock using piezoelectric and triboelectric hybrid mechanism for healthcare and sports monitoring," *ACS nano,* vol. 13, pp. 1940-1952, (2019).

[147] I.-W. Tcho, W.-G. Kim, S.-B. Jeon, S.-J. Park, B. J. Lee, H.-K. Bae*, et al.*, "Surface structural analysis of a friction layer for a triboelectric nanogenerator," *Nano Energy,* vol. 42, pp. 34-42, (2017).

[148] G.-G. Cheng, S.-Y. Jiang, K. Li, Z.-Q. Zhang, Y. Wang, N.-Y. Yuan*, et al.*, "Effect of argon plasma treatment on the output performance of triboelectric nanogenerator," *Applied Surface Science,* vol. 412, pp. 350-356, (2017).